SCHOOL OF INDUSTRIAL AND INFORMATION ENGINEERING

MASTER OF SCIENCE IN AERONAUTICAL ENGINEERING

Evaluation of SLS-made PA12 Under Uniaxial Tensile Test

Supervisor:
Prof. Alessandro AIROLDI

Alican TAŞ
842347

Academic Year 2017/2018

ACKNOWLEDGEMENT

I am appreciated to Prof. Alessandro AIROLDI for giving me the chance to perform this unique research, teaching me the strategy of methodology to reach the goal, supporting me for the better, and his effort and time on this thesis.

I owe my deepest gratitude to Dr. Alessandro GILARDELLI for his great patience, his cooperativeness and unlimited support on my thesis.

The last but not the least, I would like to thank warmly to my family and friends who provide me an unfailing support and continuous motivation in all moments of my life.

Thanks everything what makes the life good.

"Our true mentor in life is science."

Mustafa Kemal ATATÜRK

TABLE OF CONTENTS

LIST OF FIGURES

LIST OF TABLES

ABSTRACT

The morphing structures provide a development in aero field applications and they are being a realistic imitation of nature over time, bringing good efficiencies in many factors with respect to the conventional methodologies. On the other hand, these structures have some not-well predicted behaviors with new material applications. Polyamide 12 (PA12) is one of these new century materials manufactured by one of unconventional technologies, namely Selective Laser Sintering (SLS). Based on the morphing structures, the hexachiral and hexachiral tessellation morphologies are two of the in-demand researches not only in aero field but also in many other fields. As a sub-field of these researches, out-of-plane and in-plane crashworthiness of the hexachiral morphologies are being a great subject to be examined. Moreover, even there are many researches belong to out-of-plane crashworthiness, solely a limited number of resources for in-plane behavior can be found in literature.

As a study case which tries to lighten up the material characteristics by considering in-plane behavior for further, SLS-made of PA12 specimens are subjected to uniaxial tensile tests in the current thesis. The main parameters were the orientation of manufacturing of the specimens which are produced in perpendicular orientations, and four different strain rates, namely one quasi-static and three dynamic conditions. The results showed that the Horizontal orientation represents the material specifications for the aim of usage in aero field better than the Vertical orientation. In dynamic tests, materials showed brittle behavior. With increasing strain rate, specimens have reached to UTS at relatively lower strains. However, for a consistent comparison of yield stresses, it is needed to perform more tests per each specimen. Furthermore, the numerical correlations are completed successfully.

1. INTRODUCTION

1.1. CHIRAL STRUCTURE

Nature has a flawless ecosystem and every human-made structure has a story in behind which is belonging to nature. Most of the optimization problems show that the inspired technologies from the nature give better solutions from the basic attempts. Morphing structure can be regarded as a kind of imitation of nature. While the term ‘morphing’ can be introduced as capability of a structure to change its shape and size progressively during operation, the ‘morphing structure’ can refer to seamless shape changes which are continuous and different from discrete systems adopted in aerodynamic structures. This concept increases efficiency in terms of resulting forces and controllability of structures compared to the discrete ones such as flaps and ailerons. Up to day, a wide variety of solutions have been developed to provide better optimizations for adaptive capabilities of blades and wings in aeronautical field.

Nowadays, morphing structures are coming into the center of interest of the researchers, due to many concerning reasons like the availability of new concepts and smart materials, and increasing demand on the controllability of aerodynamic forces of lifting bodies. It can be said that on the target of developing the existing technology for aeronautical field, the main concern of this study takes ‘chiral topology’ into focus and evaluates the material feasibility.

The idea belongs to chiral topology shall be explained by introducing the auxetic response of materials. The materials or structures expand laterally under uniaxial tension or contract transversely under uniaxial compression. Therefore, these properties represent the material with negative Poisson’s ratio which involves high in-plane shear

stiffness and an inherent resistance to local shape variations [1] [2]. As opposed to classical sandwich constructions, the desired flexibility in the wing is obtained through the in-plane properties of the chiral honeycomb, and not using the out-of-plane properties.

Chiral topologies have characterized by overall auxetic response and offer very effective morphologies for the lightweight applications of aerospace components and structures. Conceptually, there are different chiral topologies that are used in different studies, can be seen in [3] . Particularly, the concerning chiral topology consists of *hexachiral lattices, made up of circular rings each of them connected to its neighbors with six ligaments tangent to the ring itself* [4] (see Figure 1-1).

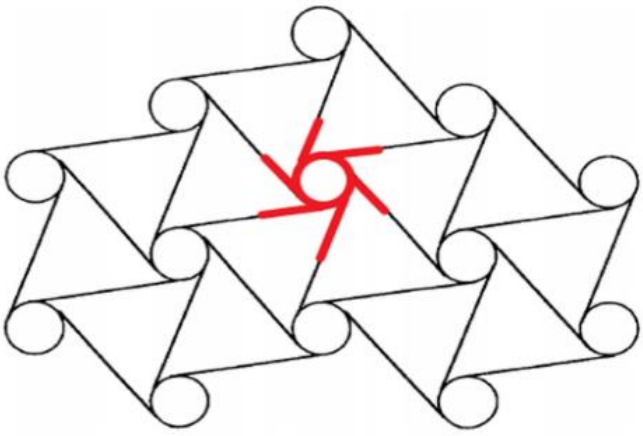

Figure 1-1 *Hexachiral Morphology*

The technological processes for hexachiral geometry was the subject of previous studies, as it is designed in [5, 6, 2] and improved in [7, 8]. As an overview, the chiral cell network as the assembly of thin ligaments and nodes will be introduced briefly by following paragraph.

In Figure 1-2, the main geometrical parameters can be sorted as R, L, r, θ, β, t_b and t_c which denote the distance between the node centers, the length of ligament, node radius, the internal angle of chirality, the angle between ligament alignment and intersecting imaginary line through center of nodes that are connected by that ligament, and thicknesses, respectively.

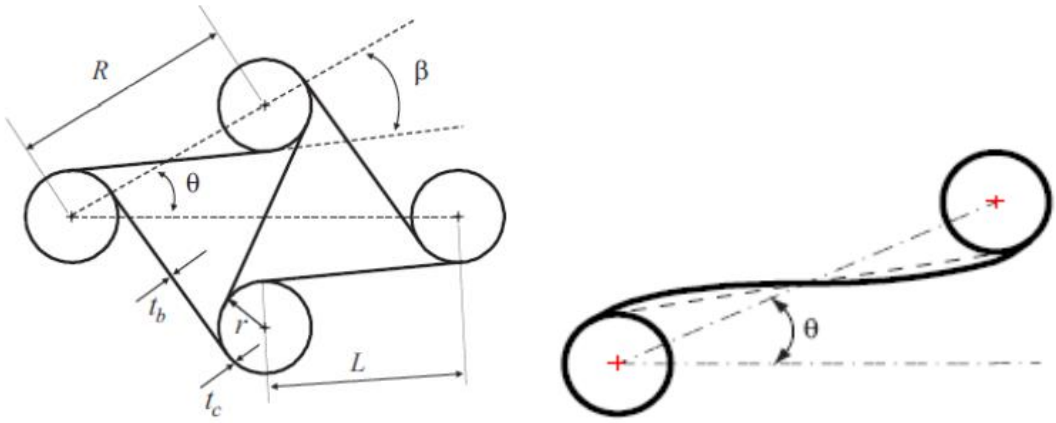

Figure 1-2 *A hexachiral structure; nodes, ligaments and some important parameters*

Different manufacturing approaches have been adopted for the production of chiral structures up to day. A technological approach for manufacturing of a composite chiral cell network has been performed by Bettini et al. [7]. In this study, they have used laminated carbon epoxy fabric plies with lay-up $[0]_5$ with a node wall thickness t_c = 1.4 mm and a ligament wall thickness t_b = 0.8 mm in all considered configurations. A special mold has been manufactured to obtain the central nodes by superposition of the curved ends of ligaments and a kind of silicon rubber has been poured into the mould to form the elastomeric inserts. The main consideration the elastomeric inserts was to exert a pressure on the adherents during bonding process. Under the specified conditions, they have applied tensile and compressive test conditions to the this assembled structure to identify strength and weak points. In both experimental evaluations and numeric results, it has been shown that the bonding is the actual weak point of the assembled structures in tension and bending failure of ligaments in compression.

Like the aforementioned study, in the study of Airoldi et al. [2], two sets of ligaments were produced by using Carbon-reinforced with lay-ups $[0]_3$ and $[0]_8$ and E-glass reinforced fabrics with lay-ups $[0]_{17}$ and $[+45/-45]_{5s}$. The stiff units made of carbon and glass reinforced ligaments have been tested until tensile failure. In both cases, the reason of failure was debonding in nodes like it is experienced in [7].

Bornengo et al. [9] have proposed a study for hexagonal chiral structure as a truss core for adaptive wing box configurations in which the hexagonal chiral honeycomb has

been used to design a race car wing with passive self-adaptive characteristics. The chiral cellular is made of ABS plastic (Acrylonitrile butadiene styrene, a thermoplastic polymer) because of its broad usage in rapid prototyping applications as an alternative way for production of honeycomb structure. The proposed configuration needs for further investigations to completely define the dependency of the in-plane linear and non-linear mechanical properties of the honeycomb versus the internal cell angle parameters.

The flatwise plastic buckling behavior of both hexachiral and tetrachiral honeycombs is evaluated by Miller et al. [10] For each type of the honeycomb structures are additive-manufactured by selective laser sintering (so called SLS) method and are made of nylon powder. In addition to finite element method (so called FEM), the tests have been done with the samples whose mechanical characteristics are organized as the relevant standards recommend for compression and shear scenarios. They have resulted the study by getting these opinions; shorter ribs and thicker walls tended to increase the maximal load before buckling onset and the absolute stresses reached for hexachiral honeycombs are higher than those reached with tetrachiral ones.

Some sort of technological processes has been proposed with a novel configuration by Airoldi et al. [8] It is stated that the existing issues of the technological developments in manufacturing of honeycomb with non-centrosymmetric topologies cannot be easily detected. In this respect, some additive manufacturing techniques have been used to produce different types of polymeric chiral honeycombs. However, many of the studies have been performed within this framework showed that mechanical properties of such materials could not meet acceptably with desired requirements of the aerospace field. From the studies [7] and [11], it has seen that there is a risk of ligament debonding as a weak point even the manufacturing of the chiral structure successfully accomplished and starting from this point of view in [8], an innovative chiral network, namely hexachiral tessellation created by adjoining polygonal shapes, has been proposed.

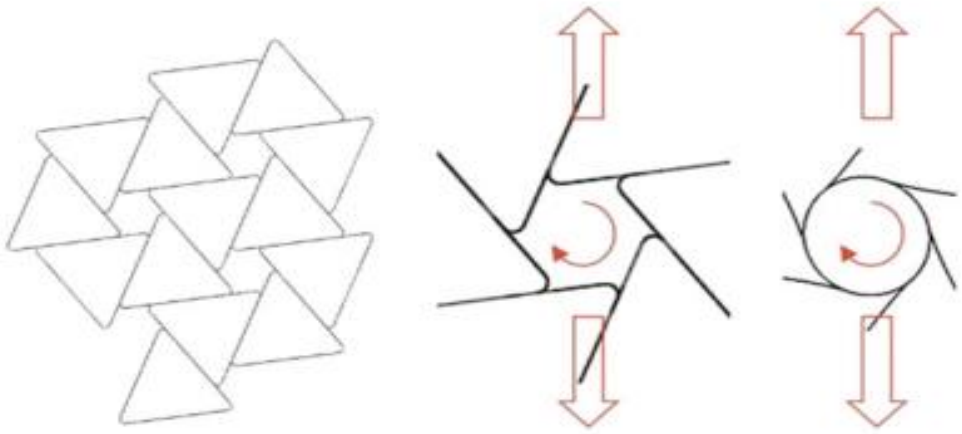

(a) *(b)*

Figure 1-3 *Hexachiral tessellation (a) and the comparison with conventional hexachiral morphology under tension (b) [8]*

The chiral networks made of carbon-reinforced and E-glass-reinforced fabrics were subjected to both tensile and compressive tests. As an evaluation of this study, the weakest points were represented by the cusps at the junctions between the external triangles because those are not protected by any reinforcement, and by reason of any hexagonal nodes do not exist at the lateral boundaries. The proposed structure demonstrated in both experiments and numerical analysis that quite accomplished auxetic behavior can be achieved.

1.2. CRASHWORTHINESS OF CHIRAL STRUCTURES

As a general definition, crashworthiness can be summarized within one sentence as the ability of structures to protect their occupants upon impact mainly by absorption of the energy. From this point of view, it naturally comes to mind that the structure shall be able to resist the external impact, and this brings the focal point of the researches onto the most durable direction of that structure. Up to day, most of the investigations have been performed by focusing on the chiral structures had paid attention on dynamic crushing behavior on the out-of-plane directions because of the fact that the out-of-plane orientated behavior of energy absorption of the structure is much more accomplished than in-plane orientated behavior. In literature, there can be found many researches interested within many aspects of the out-of-plane behaviors while the in-plane behavior

is mainly focused on in-plane elasticity. Nevertheless, there are very limited number of studies based on the in-plane crashworthiness of hexachiral tessellation structures have been performed and one of these novel studies is currently continuing in Department of Aerospace Science and Technology in Politecnico Di Milano. Since the number of studies based on the in-plane crashworthiness are limited, some systematically similar studies will be introduced.

The in-plane elasticity of auxetic honeycombs apart from hexachiral structure has been addressed in some several studies. In the research of Alderson et al. [12], 6 types of chiral honeycombs (see Figure 1-4) are subjected to tensile loading in finite element simulation while on the side, re-entrant anti-trichiral honeycomb manufactured from an acrylic sheet was tested in uniaxial compression along the in-plane x-direction to verify the FE model. The corresponding Poisson's ratio and Young's modulus values evaluated from the slopes of the transverse strain vs axial strain and axial stress–strain curves.

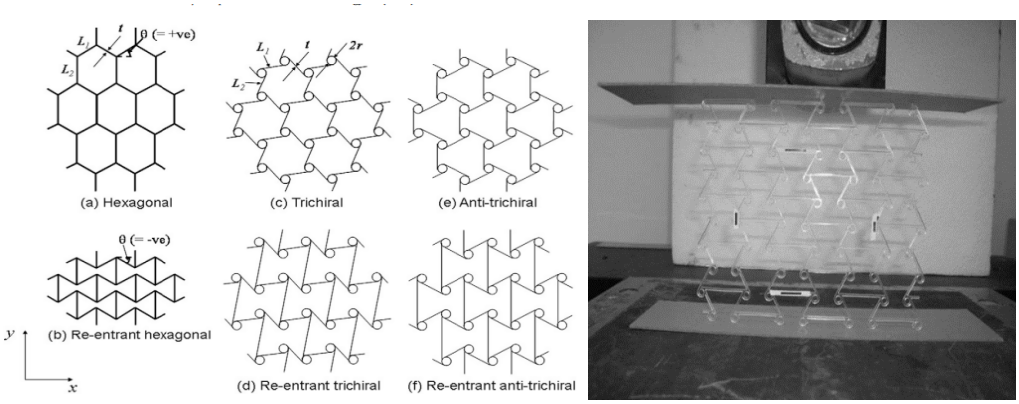

(a) *(b)*

Figure 1-4 *The identified structures (a) and the uniaxial compression test along the in-plane x-direction (b) [12]*

In another research of same author [13], this time an investigation onto 5 different type of chiral structures (see Figure 1-5) has been performed. Like in the previous study case, FE models of these structures have been supported by experiments. The samples made of Nylon powder of Duraform® were tested under compression as corresponding honeycomb structure. Poisson's ratio and Young's modulus values once again are subjected to evaluation. It has seen that the applied compressive load generates a torque which causes a rotation on cylinder nodes and bending on linked ligaments.

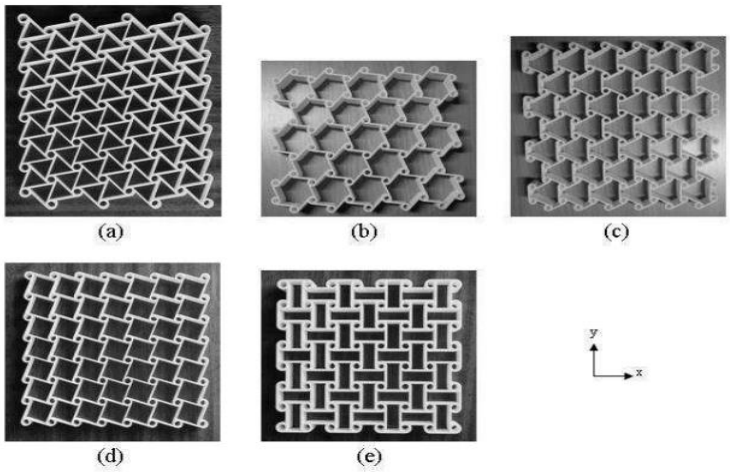

Figure 1-5 *The honeycomb structures that are used in [13]*

In [14], Zhang et al. proposed a novel quadri-arc multi-cell honeycomb (see Figure 1-6) by performing a serious of numerical analyses on dynamic behavior and energy absorption properties under in-plane impact loadings. In details, throughout the FE and experimental models, deformation modes under 3 different impact velocities including quasi-static mode, transition mode and dynamic mode, dynamic impact response and energy absorption property of the Aluminum made of quadri-arc honeycomb were examined within these brief titles by comparing a regular circular honeycomb. Consequently, it is shown that the advantage is losing out with increase of impact velocity and the quadri-arc honeycomb becomes a better choice compared to the regular circular.

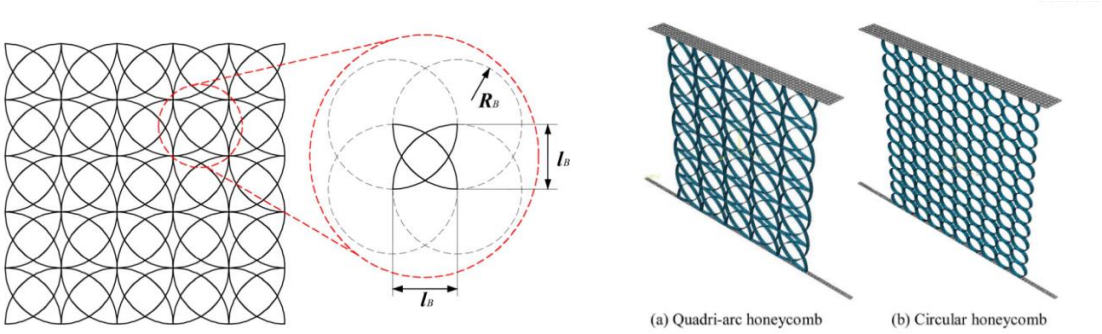

(a) *(b)* *(c)*

Figure 1-6 *A novel quadri-arc multi-cell honeycomb (a) and under in-plane impact test sturctures for quadri-arc multi-cell (b) and circular (c) honeycomb [14]*

A finite element study for in-plane dynamic crushing behaviour of hexagonal aluminium honeycombs was the subject of the research of Ruan et al. [15], by discussing the influences of cell wall thickness and impact velocity on the deformation modes. As a different manner from the previous studies, S.D. Papka and S. Kyriakides have released two interrelated articles [16, 17] for biaxial in-plane crushing of honeycombs. A special type of biaxial testing facility developed and has been used for biaxial crushing experiments of polycarbonate circular honeycombs to discuss the characteristics of force displacement responses in the first publication, while in the second publication finite element simulations of the crushing responses are dedicated to compare with the experimental results from first part. The hexagonal circular cells of honeycomb structure are compressed uniaxially and biaxially. In FE model, 6 constant strain rate tests were conducted at rates ranging from 10^0 - 10^{-5} [s^{-1}] which closer to the range the strain rates of the deformations in the lateral crushing experiments. As it is stated, the numerical simulations of biaxial crushing are able to successfully predict the major material parameters of interest.

As a last review of some other previously done researches, '*In-plane crashworthiness of chiral honeycombs'* research of D. Gao and C.W. Zhang in [18] will be looked closer. As it is stated quite clearly, the energy absorption mode of crushing honeycomb structures is rowing over each other in the in-plane directions. In this study case, the authors have spent effort in the investigation by considering effects of geometric parameters and impact scenarios such as L/R, ratio of t_b to t_c from the Figure 1-2, impact velocity and mass on crashworthiness parameters of chiral honeycombs including total and specific energy absorption or Crush Force Efficiency (CFE). As a similar manner to Figure 1-4, the fixed boundary conditions of the bottom nodes and constant velocity crushing on the top of the honeycomb structures are applied successfully with the aid of two rigid walls in FE model by constraining all of out-of-plane degrees of freedom of nodes. 5 different topology parameters L/R are investigated while the L is kept constant and 6 configurations of chiral honeycomb of L/R = 0.7 with different number of node elements and ligament elements are simulated under an impact scenario of fixed impact mass and impact velocity. It is proposed that increasing value of L/R usually result in increments in maximum impact force and total energy absorption.

Force displacement curve for different impact velocities with fixed impact mass has shown that impact force is being small and relatively independent of impact velocities when the structure is subjected to low velocity impact loading but on the other hand when the deformation arises to certain value, the impact forces increases. Lastly, it is also predicted that under a present impact velocity, the impact force of chiral honeycomb is independent of impact mass in given range.

From this moment, it may be better to mention about the method of the manufacturing with corresponding material for the present study.

1.3. SELECTIVE LASER SINTERING

In recent decades, the advanced capabilities in machinery, materials, and software have made additive manufacturing (so called AM) and rapid prototyping (so called RP) accessible to a wider range of businesses, enabling more companies to use tools previously limited to a few high-tech industries.

As an AM layer technology, Selective Laser Sintering is one of the first AM techniques, developed in the mid-1980s. SLS offers many advantages for non-mass production and customized and highly complex parts. The production technique can be summarized by following. SLS uses laser beam to sinter the materials, such as polyamides, polycarbonates, polystyrenes and recently poly(ether-ether-ketone) [19, 20]. From a CAD data, the laser beams are used to locally liquefy and fuse the pre-heated polymers in powder bed. The purpose of preheating of powder bed is to minimize thermal distortion and facilitate fusion with the previous layer in inert gas medium. [21] The unfused powder supports the part during manufacturing and eliminates the need for dedicated support structures. The platform comes down by one layer into the build chamber and the next layer is drawn on the part by a cylinder/roller. The overflow cartridges collect any excess powder that the roller did not deposit in the part cylinder (see Figure1-7). The laser then scans the next cross-section of the build and this repetition continues till the desired 3D shape is reached. After sintering phases, the platform is slowly cooled to room temperature to avoid possible shrinkage and distortion of the final product.

An important aspect is the recycling of used and unused powders after a production of desired product by SLS. Goodridge et al. [22, 23] argued in their researches even if a tiny product needs to be made, a large amount of powders is deposited in powder bed. The powders, which remain on the platform and do not contribute to the mass of the product still go through thermal cycles due to the heat generated by scanning action and attached heaters. This leads to deterioration of the properties of the powders and the property of the product made from them is no longer guaranteed. Consequently, used powders are no longer as befitting and valuable as unused powders. In the following research, Kumar et al. [24] have included recommendations of EOS GmbH company. The used powders might be mixed with 30-50% of unused powders and can be processed a few more times before the powders turn into waste. The fact might be taken into consideration that the waste powder of these materials is of high value and shall not be considered as equal to the waste of daily used, low value plastics since the cost of production and also material itself is expensive, and the process is time consuming and energy intensive. Bases on this idea, if these waste powders are not again utilized in their powder form then the energy efficiency of the SLS is critically compromised.

The mechanical properties of the parts produced by SLS are comparable to that of injection molded parts allow for end-use applications [23] while the parts made of aforementioned polymers usually possess lower mechanical properties than the parts produced by conventional methods due to the existence of small portion of porosity [21]. The comparisons between conventional injection moulding and SLS have shown that up to 1,000 parts SLS is more economical in terms of costs [25].

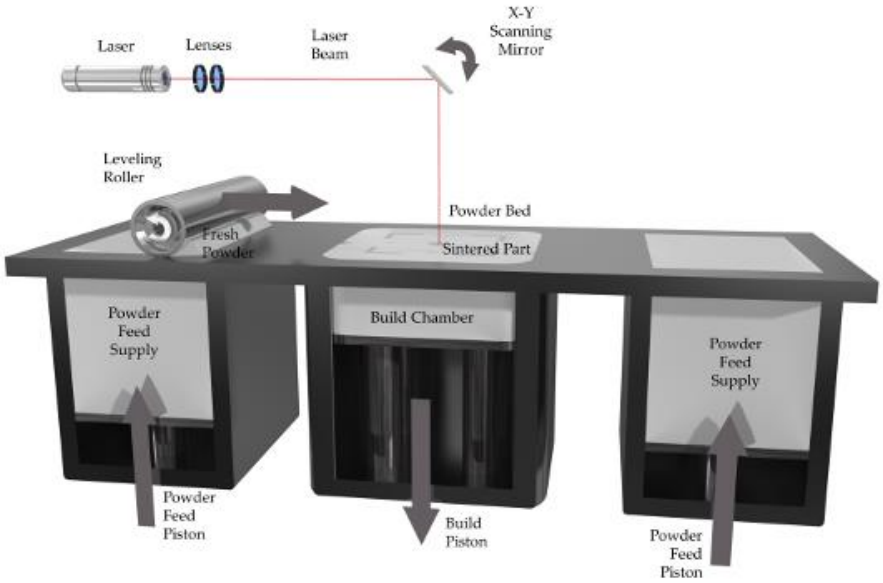

Figure 1-7 *SLS Machine visualization [26]*

At this point, it may be better to underline a basic difference with similar AM technologies, namely Direct Metal Laser Sintering (so called DMLS) and Selective Laser Melting (so called SLM). The term 'sintering' describes particle fusion processes below melting temperature, thus the process SLS is performed under the melting temperature of powder. In comparison with SLS, the main difference of DMLS can be briefly stated as the process uses fine metal powders to produce metal prototypes and tools. On the other hand, SLM uses a high-energy fiber laser which locally melts the fine metal powders. Unlike SLS, the temperature is not under melting temperature but exactly at that temperature.

Up to day, unfortunately the researches and the proposed solutions belonging to SLS-made polymers could not have a high percent compared to the conventional manufacturing methods in literature since this field is relatively new. In some researches it has seen that the quality of mechanical properties of polyamide parts produced by SLS depend on many variables such as powder bed temperature, compositions of powder, additions to powder, speed of test etc. but mainly different laser energy densities [27, 28, 29, 30] and orientation of production on powder bed [29, 31, 32, 33, 34, 35, 36, 37].

1.4. POLYAMIDE 12

Polyamide 12, as acronym PA12 or Nylon 12, is an environmental friendly polymer material with basic chemical formula of $[NH_2 - (CH_2)_{11} - CO]_p$. Nylon, as a classification, falls under the category of polyamides which include both natural substances and synthetic materials like thermoplastics. Nylons today are one of the most widely used materials for traditional thermoplastic manufacturing after their first commercial usage in 1930s. The material is generally known as its own appreciated stiffness and strength values compared to counterparts. The number after PA or Nylon simply indicates the number of carbon atoms in the material, as the reader also can see some other types in industry.

In literature, there can be found some tensile test performances by using specimens made of Polyamide varieties with different test speeds even they may be aiming some results for different research topics. As a general overview of the previous studies, some of the researches are going to be summarized by following.

In the research of R.D. Goodridge et al. [22], the effect of long-term ageing on the tensile properties of SLS-made and injection moulded specimens made of Duraform® PA12 has been evaluated. In special conditions, the ageing of PA12 has been investigated in a long-time period and for this research, standard 384 tensile test samples in upright orientation which as known to have the lowest tensile strength were produced in accordance with the standard ISO 527-2:1996, 1A. The tensile properties, namely Young's Modulus, ultimate tensile strength (so called UTS) and percentage elongation at break were evaluated using the test machine by adopting a cross-head speed of 5 mm/min. The results suggested that SLS-made PA12 samples were less affected by moisture or water absorption than injection moulded samples and appeared to hold their strength at higher temperatures better than injection moulded samples.

B. Caulfield et al. [29] have proposed a research on some build parameters in SLS process. The research focused on the effects of varying the energy density generated by laser and the influence of the build orientation by expecting that these parameters have a significant influence on the physical and mechanical properties of produced specimens. In this research case, Duraform® PA12 has been used and the test specimens and the mechanical properties were designed with respect to the ASTM D638-00 standard. Two

groups of different part build orientations have been prepared, namely orientated at 0◦ (longest axis built parallel to the x-axis), and at 90◦ (longest axis build parallel to the z-axis). The stress strain curves obtained for parts built at various energy density levels revealed that (for the parts build at higher energy density levels) the 0◦ orientated parts had higher strength and modulus relative to the 90◦ orientated parts. The yield strength for 90◦ orientated specimens exhibited a great dependence on the energy density level than for 0◦ orientated specimens. For entire energy density range tests, the 0◦ orientated parts had a greater fracture strength and less elongation at break than the 90◦ orientated parts.

Another research on the build parameters of SLS process and the consequential results has been performed by Eva C. Hofland et al. [34]. In this case, the mixture of 50% virgin and 50% used 'PA2200' PA12 powder of EOS GmbH company has been used to build specimens on 0◦ and 90◦ orientations. All 480 tensile test samples were prepared as stated in ISO 527-2 and the tensile properties were determined at 5 mm/min strain rate. Analysis of the tensile properties demonstrated that the increasing energy input has directly proportional effect, and are directionally dependent.

In this research of N. Lammens et al. [36], four different types of tests, namely tensile, compression, shear and relaxation tests have been performed to determine the entire visco-elasto-plastic response of the 'PA2200' PA12 material of EOS GmbH company, produced in the same percentages with previous research. The plastic and viscous effects are often neglected as the focus of the research is on the influence of the printing process rather than on the material response, they have proposed a deep study on mechanical performance of SLS-made of PA12. For tensile testing, the samples are designed according to specification ASTM D638 Type-III and manufactured in three directions, namely flatwise, edgewise and upright relative to the powder bed. There were three strain rates preferred as the cross-head speed of the test machine, namely 5, 50 and 500 mm/min. From the engineering stress-strain curves for the different manufacturing orientations and tests speeds, a slight increase of Young's Modulus with increasing test speed and an increase in the plastic strain hardening with increasing test speed is confirmed. UTS was higher for edgewise and flatwise samples and stretch of these samples were almost doubled as compared to upright samples and these are attributed to

the favorable orientation of the manufacturing layers to the tensile loading direction in these samples. Increasing the test speed results in an overall increase of UTS over all samples as a consequence of the visco-elasto-plastic response of PA-12.

Another research [37] on the manufacturing orientation of parts SLS-made of PA12 of Duraform® has been investigated by tensile, flexural, and compression testing methods to assess the changes in the mechanical properties. The tensile testing specimens are manufactured in x, y and z axis build orientations relative to the powder bed with five samples in each orientation by considering ISO standards. A test speed of 1 mm/min was used to determine the tensile modulus and after the rate was increased to 5 mm/min to measure the UTS. The mechanical properties are served in a table with respect to manufacturing orientation, and referred table has been used also in some other research articles. UTS and tensile modulus have found as the highest in x orientation, while the elongation at break value has also shown that the x orientation gives the best compromise.

In this thesis, the idea of the study comes from previously presented four titles. As it is mentioned earlier, there are some researches exist in the Department of Aerospace Science and Technology of Politecnico di Milano and the group of researchers are interested in the in-plane crashworthiness of hexachiral structure which is SLS-made of PA12 of EOS GmbH company. As a complementary work of aforementioned research, to check and understand better the required characteristics of the material, the specimens are subjected to uniaxial tension loading under the displacement controlled test conditions with changing strain rates, namely in quasi-static and dynamic conditions.

2. METHODOLOGY

2.1. SPECIFICATIONS

Naturally, there are some methods to investigate the tensile behavior of materials by using specified test specimens and to define the properties of specimens and test conditions are standardized by several internationally accepted and well-known specifications. Determination of tensile properties of concerning material of this study can be supplied by ISO 527-1:2012[1] and ISO 527-2:2012[2] released by International Organization for Standardization in 2012 and ASTM D638-14[3] and ASTM D882-12[4] released by American Society for Testing and Materials in 2014 and in 2012 respectively and kept updated by 2018. ISO 527-1:2012 and ASTM D638-14 address the same subject matter with some sort of differences in technical contents for the determination of tensile properties of plastics. Even all of these are technically equivalent resources, relatively, they cannot provide completely comparable results because of the facts that their methodologies and advices on shape formation differ in some respects. As a general acceptance in both standards, specimens have *'dog bone'* shape with various dimensions.

By the following paragraph, there will be explanations and comparisons for different methods in some respects. A main differentiation starts with the thickness size of the specimens. It is recommended to select ASTM D638-14 standard for the specimen thickness up to 14 mm while ASTM D882-12 shall be preferred for thin sheets which

[1] ISO 527-1:2012 Plastics -- Determination of tensile properties - Part 1: General principles
[2] ISO 527-2:2012 Plastics -- Determination of tensile properties - Part 2: Test conditions for moulding and extrusion plastics
[3] ASTM D638-14 Standard Test Method for Tensile Properties of Plastics
[4] ASTM D882-12 Standard Test Method for Tensile Properties of Thin Plastic Sheeting

has less than 1.0 mm in thickness. Similarly, such differentiations can be seen for various thickness values in corresponding title and annexes of ISO 527-2:2012. The preference has been done in pursuant of 1.0 mm thickness of the material.

However, the exact stress-strain characteristics of plastic materials are highly dependent on many factors and being aware of this fact, all the specimens kept in same and optimal ambient and tests applied on equal conditions except their characteristic differences like different displacement rates of cross-head of the testing machine.

2.2. SPECIMEN PREPARATION: SHAPE AND DIMENSIONS

In this study, it has been decided to have the specimens according to the rules specified within the standard ISO 527-2:2012. The provided materials have thicknesses around 1.0 mm and enough length and wide compared to the information stated by the standard. Then another most important criteria to examine strain rate of the material is the test machine speed which is limited up to a specific level. Based on the definition of strain rate, when it is remembered that one of the target of this study was to disclose the behavior of material in high strain rates as a dynamic response, the best solution is to use smaller specimens prepared within the procedure stated by standards. This is theoretically possible with aforementioned standards without any problem, but on the other hand the applicability for small sizing in real applications should be thought even the testing machine has reasonable limits.

By considering the thickness factor of specimen suggested by standard and the existing one in the hand, the specimens have been decided to create in accordance with the standard, specifically it is called specimen type 5B in the standard ISO 527-2:2012. The dimensions and corresponding technical drawing for these dimensions can be seen by following Table 2.1 and Figure 2.1. Based on the availability of enough length of the coupons SLS-made of PA12, it has been decided to have the specimens 100 [mm] in overall length by rescaling the given dimensions by the standard. It is important to remind for this decision; the fact has been taken into consideration that the advised overall length which is free to select from 35 [mm] by the standard. In the corresponding column of Table 2.1, the designed dimensions for the specimens are also served.

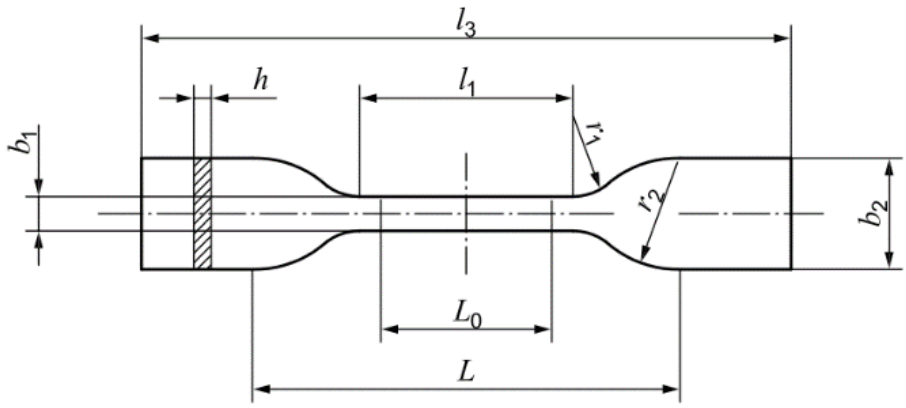

Figure 2-1 *The drawing for tensile testing specimen type 5B of ISO 527-2:2012.*

Table 2-1 *The technical specifications for tensile testing specimen type 5B of ISO 527-2:2012*

l_3	Overall length	≥35	105	[mm]
b_2	Width at ends	6 ± 0,5	18	[mm]
l_1	Length of narrow parallel-sided portion	12 ± 0,5	36	[mm]
b_1	Width at narrow portion	2 ± 0,1	6	[mm]
r_1	Small radius	3 ± 0,1	9	[mm]
r_2	Large radius	3 ± 0,1	9	[mm]
L	Initial distance between grips	20 ± 2	60	[mm]
L_0	Gauge length	10 ± 0,2	30	[mm]
h	Thickness	1 ± 0,1	3	[mm]

There were some coupons produced by the innovative tech SLS machines of EOS GmbH and they are divided into two groups according to their production orientations. The parts in one group were orientated at 0◦ with respect to X-Y plane of powder bed of SLS machine so that the widest surface of the specimen can be seen throughout the Z axis; is called *Vertical*. The other group is oriented at 90◦ with respect to X-Y plane of powder bed of SLS machine so that the widest surface of the specimen can be seen throughout the Y axis; is called *Horizontal* (see Figure 2-2).

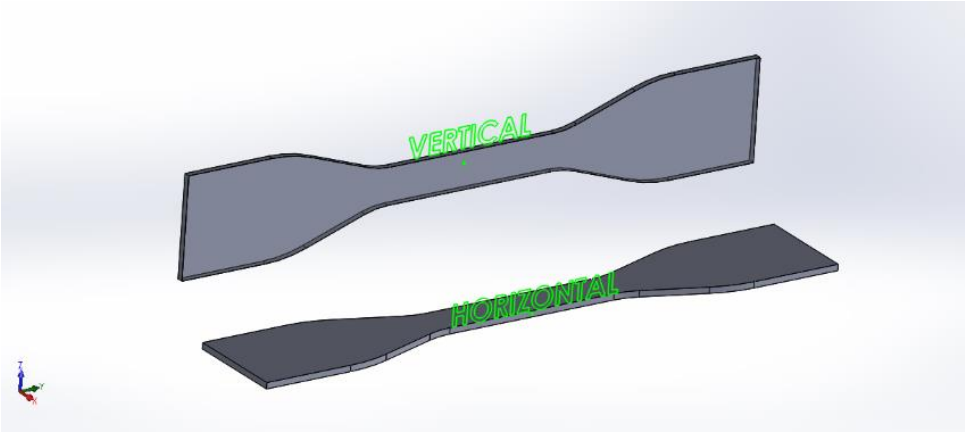

Figure 2-2 *A visualization of Vertical and Horizontal specimens with respect to the manufacturing orientation*

All the coupons were used to produce *three specimens per each coupon* within the given sizes, by treating with water jet cutting machine. In total, it has been owned 8 specimens in Vertical and Horizontal directions as an amount of half and half.

As it is going to be stated in the next chapter, the correct measurement for cross section of gage area is crucially important for numerical analyses. Due to this reason, a sort of dimension checks was performed before starting of the tests. The dimension checks were done through 3 points; at the center and 15mm away in both directions from center on gage area, and for each point the measurements have been repeated 3 times. The average of these measurements in gage area is given by following Table 2-2.

Table 2-2 *The averaged nominal cross-sectional area of the specimens in gage part*

SPECIMEN		AVERGE WIDTH [mm]	AVERAGE THICKNESS [mm]	CROSS SECTIONAL AREA [mm^2]
HORIZONTAL	***1***	6.23	1.22	7.6006
	2	5.92	1.08	6.3936
	3	5.67	1.22	6.9174
	4	6.15	1.26	7.7490
VERTICAL	***1***	5.13	1.04	5.3352
	2	5.28	0.98	5.2428
	3	5.17	1.05	5.1744
	4	5.14	1.02	5.4285

2.3. SPECIMEN PREPARATION: MATERIAL PROPERTIES

The material of the current study case is a type of polyamide 12 which is commercially known as *PA2200 Speed 1.0* of EOS GmbH company. Some important characteristics according to the field of this study for the material provided from producer can be given by following Table 2-3.

Table 2-3 *Some important material properties of current test specimens [38]*

PROPERTY	DIRECTION	VALUE	UNIT	TEST STANDARD
Tensile Modulus	X - Direction	1600	[MPa]	ISO 527-1/-2
	Y - Direction	1600		
	Z - Direction	1550		
Tensile Strength	X - Direction	48	[MPa]	ISO 527-1/-2
	Y - Direction	48		
	Z - Direction	42		
Strain at Break	X - Direction	18	[%]	ISO 527-1/-2
	Y - Direction	18		
	Z - Direction	4		
Density	-	930	[Kg/m^3]	-

Here in this point, it might be better to remind some elucidations. The rate of change of strain as a function of stress is an important consideration because the slope of the straight line in the elastic region of a stress-strain curve is called '*Modulus of Elasticity'*. It is basically an indicator of resistance of a material to being deformed elastically. The concerning type of Modulus of Elasticity, namely '*Elastic Modulus'* takes to heart the tensile elasticity.

$$E = \frac{\sigma(\varepsilon)}{\varepsilon} = \frac{P/A}{\Delta L/l_0}$$

The *Strain Rate* is the one of the most crucial parameters that has important role on the overall experiments and has the basic definition as the rate of change in strain of the specimen with respect to time.

$$\dot{\varepsilon}(t) = \frac{d\varepsilon}{dt} = \frac{d}{dt}\left(\frac{L(t) - l_0}{l_0}\right) = \frac{1}{l_0}\frac{dL(t)}{dt} = \frac{v(t)}{l_0}$$

When above equation is taken into consideration, it can be easily said that the speed of the two gripped ends of the specimen throughout the uniaxial tensile loading, i.e. the speed of the cross head of tension testing machine with respect to the fixed one, has a significant importance. In a standard tensile testing, the results of the tests are provided based on a pre-defined pull-off speed and this speed corresponds to strain rate on the specimen by dividing into the initial gage length. For the details of definitions and methods to measure and/or apply the elastic modulus and strain rate, the readers are recommended to review both standards ISO 527-1:2012 and ASTM D638-14.

Here in this step, it might be beneficial to underline that when two samples are produced with different manufacturing methods, there can be significant differences in tensile properties of these two samples. In details of Figure 2-3, if the SLS-made PA12 is compared to the conventional injection molded PA12, it can be obviously said that the SLS-made PA12 samples show better tensile strength compared to the injection molded PA12 while SLS-made PA12 ruptured at very low strain values with respect to the other.

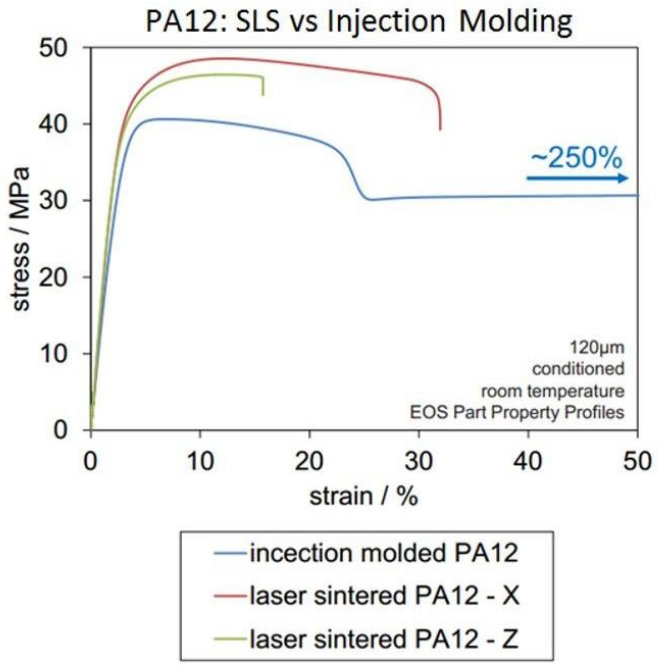

Figure 2-3 *A comparison of different PA12 manufacturing methods as stress strain curve [39]*

2.4. STRAIN GAGE MEASUREMENT

If the material has some imperfections in its way of production, those imperfections has crucial effects on the calculation of elongation and the cross-head movement includes also such mismeasurements. The manufacturing method of injection molding typically has lower porosity and greater homogeneity compared to the SLS, thus it leaves fewer imperfections in the structure of the material to encourage crack propagation. The specimens manufactured via SLS have relatively more percent of imperfections with respect to the conventional injection molding and this might decrease the accuracy of measurement. However, another respect that should be taken into consideration comes to mind. Even the testing machines are the high technology products, they require a very short period to provide the demanded velocity of the cross-heads by forcing the pistons in which the flow starts from zero to corresponding level. Consequently, this phenomenon can be interpreted as transient and the effects should be examined by comparing another method of displacement control.

Here, strain gages become a part of this study as one of the most commonly used sensors. In spite of the fact that they are giving a local measurement in gage area, i.e. not a whole measurement for overall length of specimen, this is one of the easier and cheaper method in terms of costs and time consuming by considering that it doesn't require a post processing. *L2A-06-062LT-350* type strain gages of *Vishay Micro Measurement* company are mounted into the center of gage area of 4 Horizontal and 4 Vertical specimens. The preferred type of *Tee-Rosette strain gage* provides measurement up to 50,000 microstrain. By definition, strain gage rosette is an arrangement two or more closely positioned gage grids and separately oriented to measure the strains along in different directions. Tee-Rosette is the special kind of strain gage with two gage grids to measure the strain in two perpendicular directions, namely in X and Y directions (the directions where the specimen has 2 widest lengths) with respect to uniaxial tensile testing direction if it is considered that the force is applied through X/Y direction (see Figure 2-4). The installations of the strain gages with *M-Bond 200 Adhesive* on the specimens are correctly performed in accordance with technical instructions by authorized person.

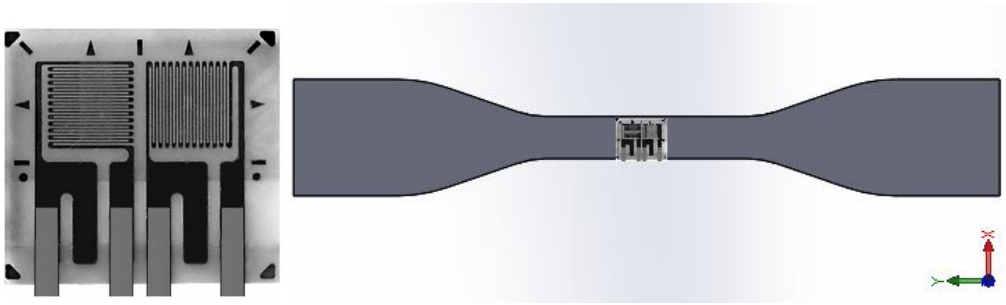

Figure 2-4 *Tee-Rosette strain gage of Vishay Micro Measurement company and installation visualization*

3. EXPERIMENTAL AND NUMERICAL ANALYSES

3.1. EXPERIMENTAL ANALYSIS

In the first part of the study, it is decided to perform a quasi-static and three dynamic tests with pre-defined varying cross-head speeds of the test machine. The pre-defined cross-head speed are same for both Horizontal and Vertical specimens and given by following Table 3-1. In the light of requirements for understanding the material characteristics, the strain rates for this complementary job are selected by partially considering what the standards recommend.

Table 3-1 *Four different strain rates applied in experiments*

TEST NO	STRAIN RATE [mm/s]
1	0.03
2	30
3	240
4	480

From now on, for a simplification for naming of each specimen, it is going to be followed these abbreviations and numbers:

- For the specimens Horizontal : H
- For the specimens Vertical : V

and,

- For cross-head speed of test #1 (quasi-static) : 0.03
- For cross-head speed of test #2 (intermediate-dynamic) : 30
- For cross-head speed of test #3 (intermediate-dynamic) : 240
- For cross-head speed of test #4 (high-speed-dynamic) : 480

Example:

Vertical specimen tested with cross-head speed *240 [mm/s]* ⟶ *"V_240"*

All the tests performed with test machine *MTS 858 Minibionix II* [40] of MTS Systems Corporation. This machine is a versatile, servo-hydraulic test machine and is an effective choice for low force static and dynamic testing machine which specifically allows to perform tensile testing for lower strength materials like PA12. To characterize better the material response to applied tensile loading, it is decided to apply first quasi-static tests and after the highest speed dynamic tests and then the other two intermediate speed dynamic tests. All the tests are recorded with *Nikon 1J5* [41] digital camera as photographs and videos. For the dynamic tests, an advanced movie option, namely slow motion, is used to capture the fast motion of test specimen up to breakage in 120 fps with 1280 x 720 frame size.

In Figure 3-1 and Figure 3-2, the specimens are shown in the moment before tests started and after the breakage occurs for Horizontal and Vertical with increasing cross-head speed of uniaxial testing machine, respectively.

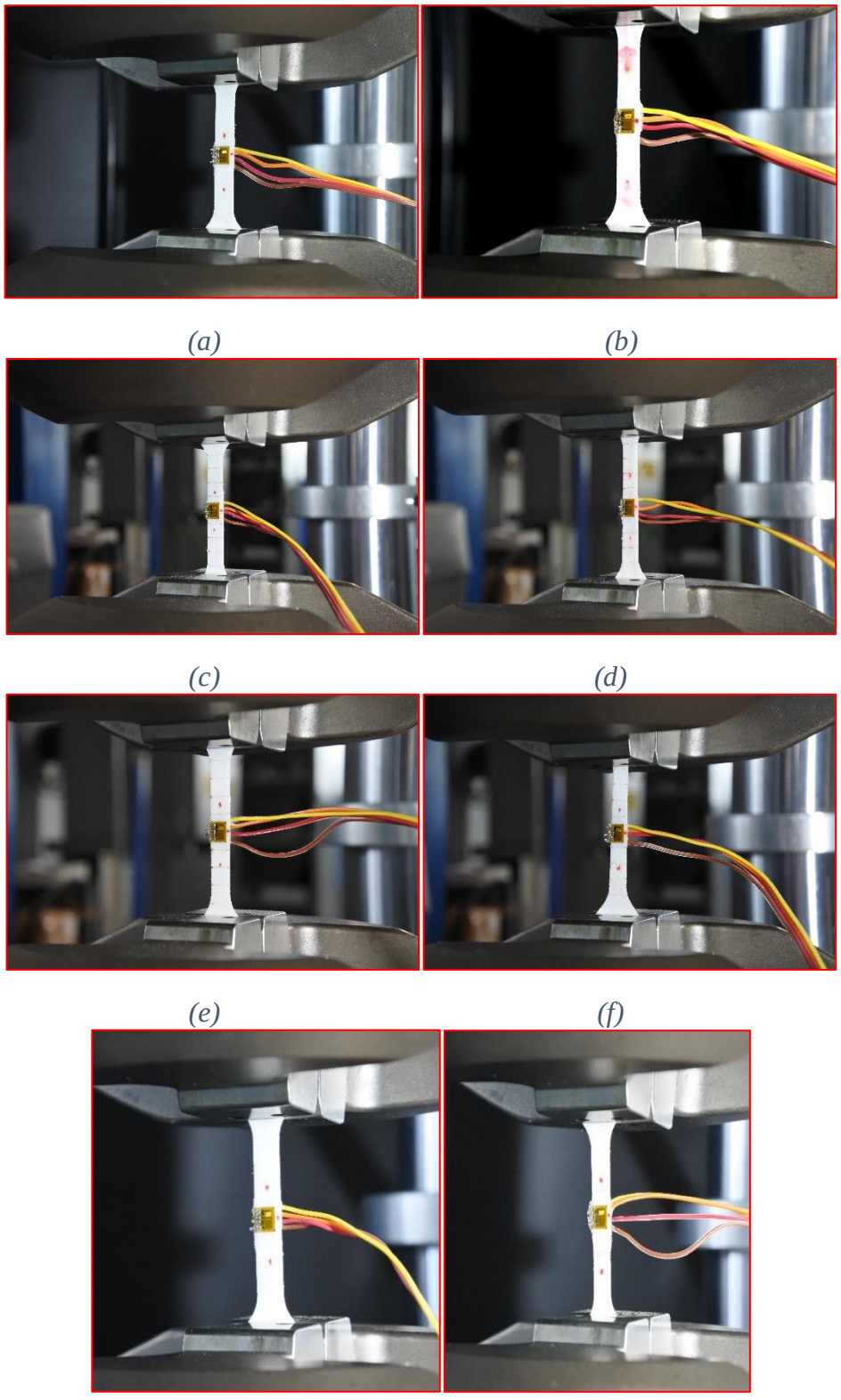

(a) *(b)*

(c) *(d)*

(e) *(f)*

(g) *(h)*

Figure 3-1 *The captures for specimens before starting the tests: H_0.003 (a), V_0.003 (b), H_30 (c), V_30 (d), H_240 (e), V_240 (f), H_480 (g) and V_480 (h)*

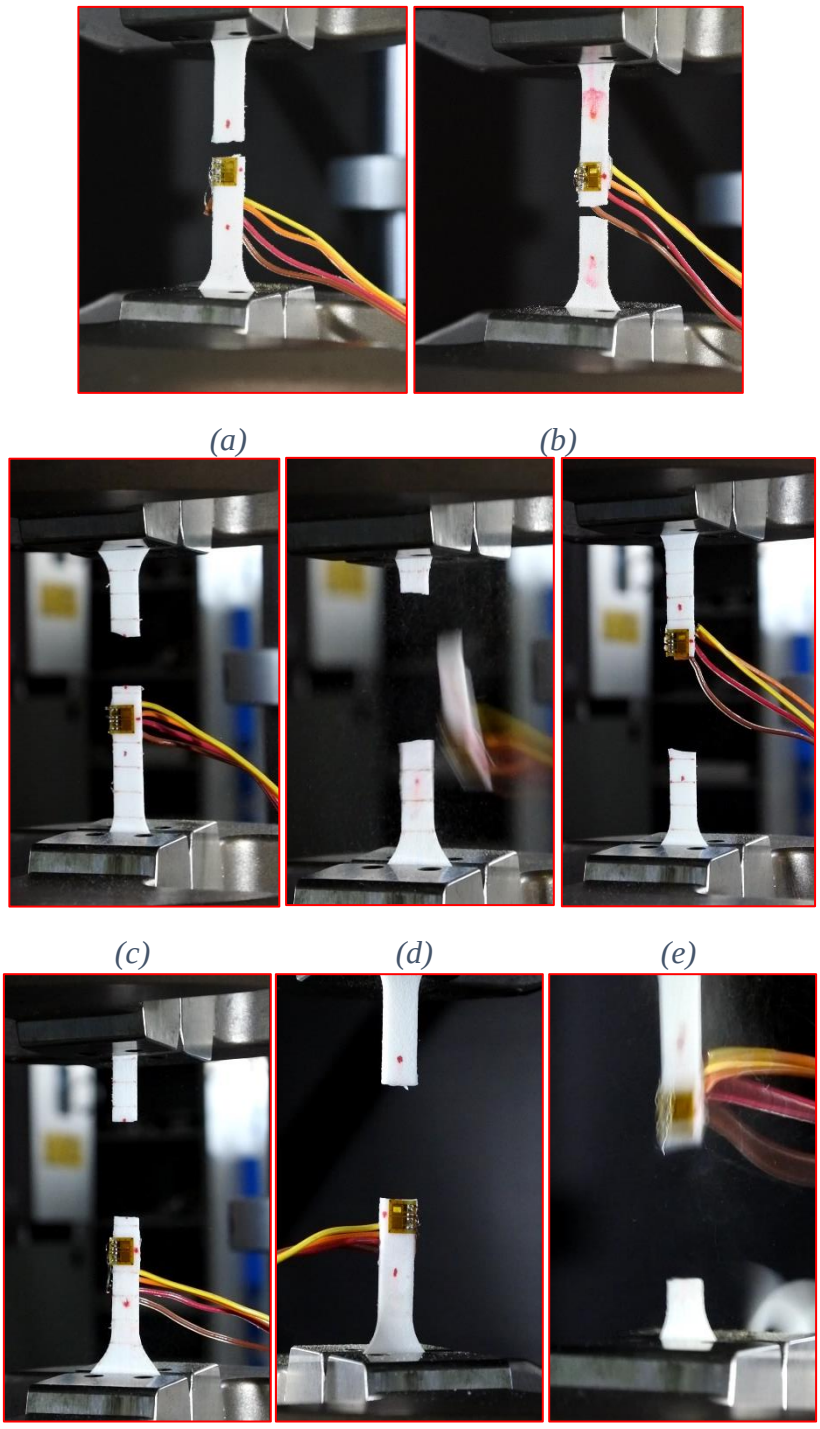

(a) *(b)*

(c) *(d)* *(e)*

(f) *(g)* *(h)*

Figure 3-2 *The captures for specimens after breakage occurs: H_0.003 (a), V_0.003 (b), H_30 (c), V_30 (d), H_240 (e), V_240 (f), H_480 (g) and V_480 (h)*

After all the test are completed, the results obtained by the aid of strain gages are withdrawn from the user interface of testing machine and processed the data like as the given example in following Table 3-2.

Table 3-2 *The data example served by user interface of testing machine*

Time	Axial Displacement	Axial Force	Est1-c1	Est2-c2
[Sec]	[mm]	[kN]	[microstrain]	[microstrain]
0.000000000	0.000000000	0.000000000	00.000000	00.000000
0.021972656	0.003142495	0.001048381	37.043045	-15.531461
...	...	...	...	...

The processed data shows clearly the applied force, corresponding axial displacement and time, while also shows the measured strain in both longitudinal and transversal directions in terms of microstrain. In this point, it might be a good decision to briefly remind that the ratio of the transverse contraction strain to longitudinal extension strain is defined as Poisson's ratio.

$$\nu = -\frac{d\varepsilon_{transverse}}{d\varepsilon_{longitudinal}}$$

As a result of this phenomenon, the Poisson's ratio for performed each test is determined based on the recommendation of the standard ISO527-1:2012, Annex B. Poisson's ratio per each corresponding time for each specimen is calculated and listed and finally the average value is served by following Table 3-3.

Table 3-3 *Specimens' Averaged Poisson's Ratio values*

SPECIMEN		**AVERGE POISSON'S RATIO**
HORIZONTAL	***H_0.03***	0.43860
	H_30	0.39809
	H_240	0.38849
	H_480	0.41751
VERTICAL	***V_0.03***	0.45696
	V_30	0.32910
	V_240	0.36522
	V_480	0.41194

The processed data have been cleared from the results recorded after breakage occurs, and then graphed by using MATLAB®. The applied force versus axial displacement through the applied force for all the specimens are given in Figure 3-3 while in the Figure 3-4 and Figure 3-5, the aforementioned graph is divided into two for Horizontal and Vertical specimens to figure out the details better.

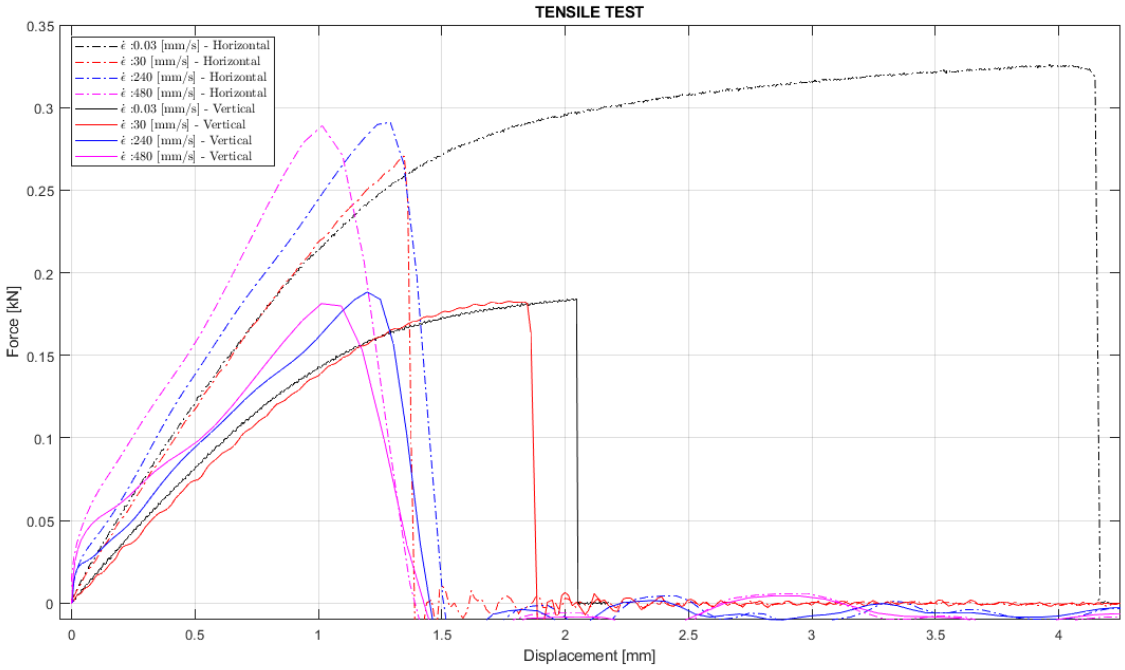

Figure 3-3 *The force applied through the specimen's longest side and axial displacement in this direction for all specimens*

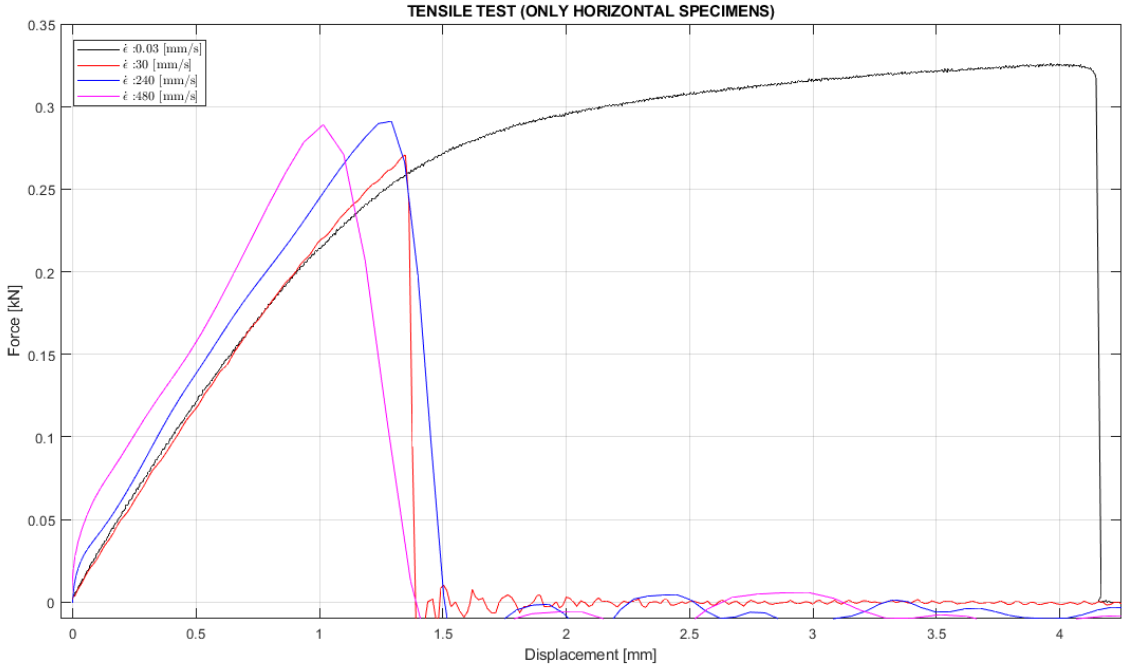

Figure 3-4 *The force applied through the specimen's longest side and axial displacement in this direction for horizontal specimens*

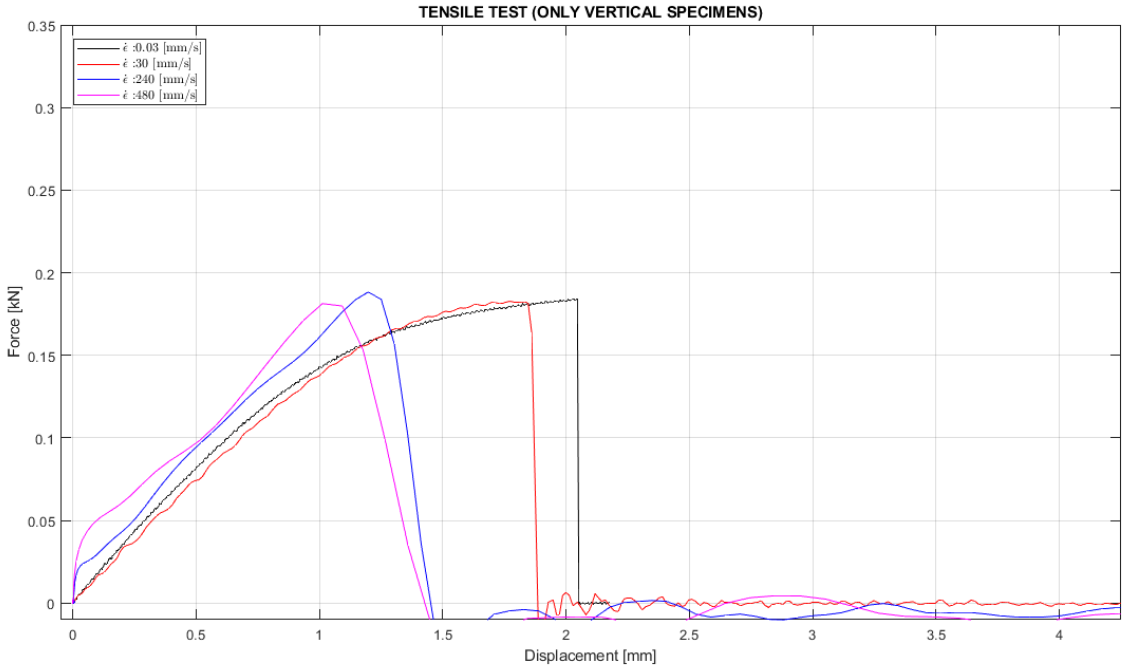

Figure 3-5 *The force applied through the specimen's longest side and axial displacement in this direction for vertical specimens*

As the first observation by considering the above three figures, it is obvious that the Horizontal specimens show significantly better strength than Vertical specimens in each test with different strain rates. In Horizontal specimens, the quasi-static test with strain rate $\dot{\varepsilon} = 0.03\ [mm/s]$ shows higher strength and much more axial elongation than the dynamic test as expected. On the other hand, the Vertical specimen with quasi-static test with strain rate $\dot{\varepsilon} = 0.03\ [mm/s]$ couldn't show the expected strength as it couldn't exhibit competitive values for the other dynamics tests with respect to Horizontal ones. In overall, for the material it can be said that brittle than expected behavior. It is considerable that being able to talk about strength, it is ineluctably useful to continue with stress-strain graphs which will be discussed in following title by considering also the numerical correlations. In the following Table 3-4, the maximum forces are applied during the tests before breakage, and the corresponding axial displacements can be seen.

Table 3-4 *The maximum force applied on all specimens, and corresponding axial displacements*

SPECIMEN	FORCE APPLIED (kN)	AXIAL DISPLACEMENT (mm)
H_0.03	0.3260	3.9631
H_30	0.2708	1.3475
H_240	0.2911	1.2909
H_480	0.2891	1.0145
V_0.03	0.1843	2.0306
V_30	0.1828	1.7745
V_240	0.1884	1.1975
V_480	0.1814	1.0118

In these three graphs, it can be easily seen some fluctuations in elastic regions. Some materials like rubbers, plastics and specifically polymers can exhibit a strong non-linear behavior from the beginning of identified curves. In fact, this situation brings to mind a linearization to predict better the overall material behavior. For this reason, an investigation for linearization of elastic region has been performed by using a simple linear regression in which the first order polynomial fits in a least-squares sense for the applied force. The details concerning the linearization will be continued to discuss in section 3.3, after introduced the numerical analysis method.

3.2. NUMERICAL ANALYSIS

Strictly speaking, only the experimental results can be misleading in the aim of finding a reliable demonstration of material behavior in tensile conditions if it is explored with respect to some comparable conditions such as the method of production and the orientation of manufacturing. For such reasons, it is decided to perform simultaneous finite element analyses with respect to experimental activities. In this study case, ABAQUS® (student version) was selected as suitable software as the source of numeric analyses.

The shape of specimens is modelled by Abaqus/CAE as a 3D deformable shell within the dimensions specified in Figure 2-1 and by considering the width and thickness values in the Table 2-2. The material properties are applied based on information released by producer and the experimental results. The section is created as a *'homogeneous shell section'* by considering the ratio of thickness to the other two dimensions. In the step definition, there were two procedures that are used throughout all the analyses, namely '*Static, General'* for quasi-static tests, and *'Dynamic, Explicit'* for all the remaining dynamic tests for both Horizontal and Vertical specimens.

Abaqus/Standard has been preferred to perform 'Static, General' procedure in the quasi-static tests. As an implicit method, Abaqus/Standard uses the Newton Raphson method to obtain solutions for nonlinear problems, it combines incremental and iterative procedures to obtain an equilibrium solution. As a general aspect, the static analysis divides the input 'displacement' into small increments and performs an incremental analysis by increasing the solicitation value, namely ramp function, by each increment. Finally, when the equilibrium solution is reached, the increment becomes completed. For each iteration, Abaqus/Standard forms the stiffness matrix of the model and solves a sort of equations to calculate the displacement correlation. From the updated configuration starting from structure's initial stiffness, the internal forces also are computed and then the difference between internal and applied force is checked. Whenever this force residual of the corresponding iteration falls down the tolerance value, the iterations stop. This methodology brings a computational cost in terms of time but compared to the other procedure, namely Abaqus/Explicit, is much more less. A quasi-static problem can also be solved with Abaqus/Explicit but requires some

considerations. A static solution is impractical to analyze the simulation in its natural time scale since it requires an excessive number of small time increments for a long-time solution, the solution must be accelerated such as increasing the speed of analysis. But in such case, the application of loading will also be affected and there will be a risk of losing the smoothness of changes, which means the analysis is not a quasi-static anymore. For this order of speeds, the solution obtained by '*Static, General'* procedure provides consistent result. It is important that it's decided to perform this type of procedure only and only in quasi-static tests by considering the consumed time to obtain the results.

As it is stated before, Abaqus/Explicit uses an excessive number of small time increments like on the order of 10^4 to 10^6, while an implicit method such as Abaqus/Standard requires fewer magnitudes of increments. Abaqus/Explicit uses the Central Difference Method to generate the equation of motion explicitly through time by using a kinematic condition in one increment to calculate the kinematic condition for next increment. At this moment, it might be useful to talk about the term '*explicit*'. The state at the end of the increment is based only on displacement, velocity and acceleration at the beginning of increment due to Central Difference Method. Based on the definition of Central Difference Method, the integration of constant accelerations is exact and so that the accurate results can be achieved with very low order time increments. Since the explicit procedure uses a diagonal or lumped mass matrix, the solution for accelerations becomes trivial and this bring the fact that each increment is inexpensive. However, when it is remembered that the order of increments is huge, this brings a substantial waiting time during the analysis period. Abaqus/Explicit is the product that is particularly suited to simulate brief transient dynamic cases such as contact conditions. In case of contact conditions, the explicit method is readily formulated with such contact conditions and the solution process will be performed with node by node basis without iteration. For further information, it is preferable to see the manuals provided by the company. The *'Dynamic, Explicit'* procedure has been applied in all dynamic cases with both Horizontal and Vertical specimens.

In the experiments, the test specimens are gripped from the both ends to the test machine, as it is known. In the finite element model, all the model is partitioned Figure

3-6 and both sides that would be gripped are modelled as '*rigid body constraints*' and the parts to be constrained are subjected to a crosscheck with the photographs taken before tests start. From the upper side (reference point RF-1 in Figure 3-6 (a)) a 'displacement control' with changing amplitudes per each test has applied while the down part of the rigid body constraint (reference point RF-2 in Figure 3-6 (a)) is assigned as encastre. As a boundary condition, it is set up to move only in loading orientation to prevent any misleading in any other orientation. As the 'field output request', the main stress, plastic and logarithmic strain, translation and rotation displacements, velocities and accelerations, and reaction forces are requested. For the 'history output request', the selected main parameters were axial displacement, reaction force and logarithmic strain in loading orientation.

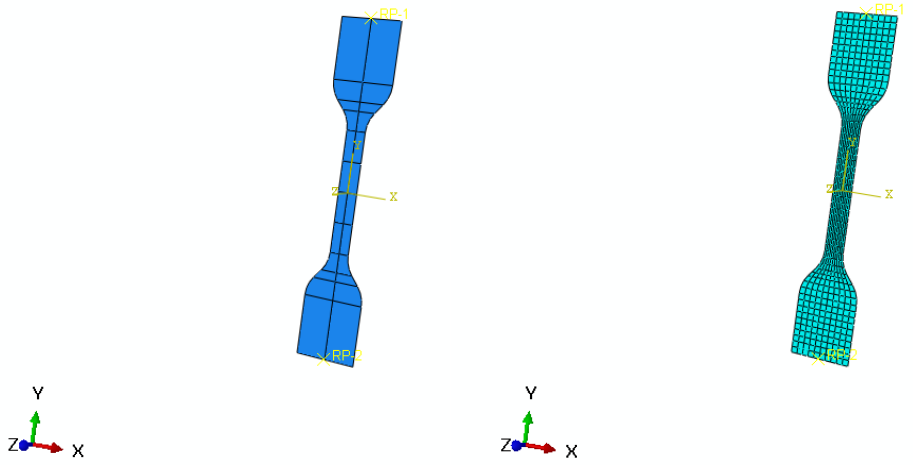

(a) *(b)*

***Figure 3-6** FEM for specimens with partitions (a) and meshed view (b)*

As a basic requirement of almost every finite element analysis, meshing has been performed within some considerations. The student version of Abaqus, released for educational use for free, has some limitations than complete set. By considering these limitations, such as the total number of nodes, approximate global sizing suggested by software itself is confirmed and then the gage area is seeded by increasing the number of elements. In the current study case, 627 nodes and 560 quadri-lateral, 4-node, stress/displacement shell elements with reduced integration and a large strain formulation, namely S4R is preferred (see Figure 3-6 (b)).

3.3. RESULT EVALUTIONS

3.3.1. NUMERICAL CORRELATIONS IN ELASTIC REGION

In section 3.1, the first order polynomial fitting has been introduced briefly but now, by adding the contribution of numeric analysis, the results will be started to discuss. The experimental results, first order polynomial fitting and numeric correlations are summed up in a graph per each specimen, as Nominal Stress vs. Displacement graph. The underlying reason of evaluation 'Nominal Stress vs. Displacement' instead of 'Force vs. Displacement' is causing from the wide range of nominal area variation that can be seen in Table 2-2. In the evaluation of stress – strain curves, this wide range of nominal area variation creates some sort of mistakes to read the graph. Therefore, to overcome of this vexing problem, it is decided to look at 'Nominal Stress vs. Displacement' curves to have the correct results for stress – strain curves. After some experiences over the results with the aforementioned problem, it is decided to perform a modification in FEMs. The mentioned modification is a kind of stress - displacement correlation in order to obtain more correct Young's Modulus per each specimen for all strain rates by modifying the cross-sectional area of specimens grouped in three sections. The specimens with higher than 7 mm^2 nominal area is modelled as 7 mm^2, while the specimens which have a nominal area between 6 mm^2 and 7 mm^2 are modelled as 6 mm^2 and similarly the others lower than 6 mm^2 are modelled as 5 mm^2. By going back to the Table 2-2, it can be summarized as the quasi-static and highest dynamic tests applied on Horizontal specimens are modelled as the first group, while the intermediate dynamic tests applied on Horizontal specimens are modelled as the second group. All the 4 specimens of Vertical specimens are modelled as third group. In all following graphs related to this part of evaluation, the experimental curves are taken as colorful up to the maximum corresponding Nominal Stress value, and then continued as light grey.

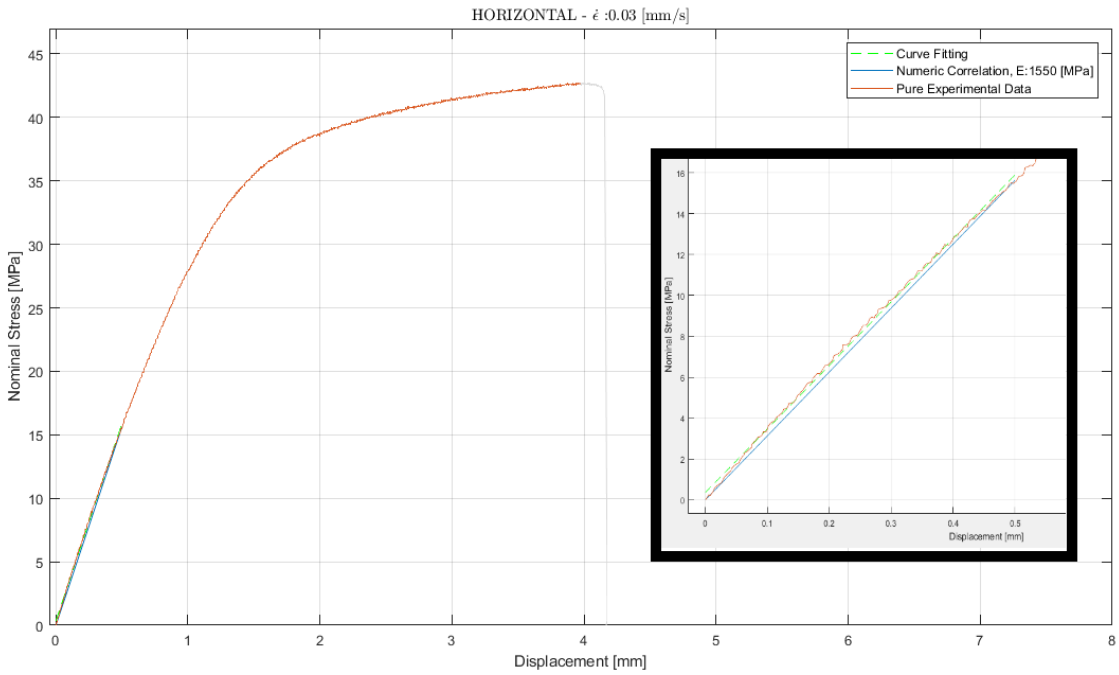

Figure 3-7 *Numerical correlation in elastic region for H_0.03*

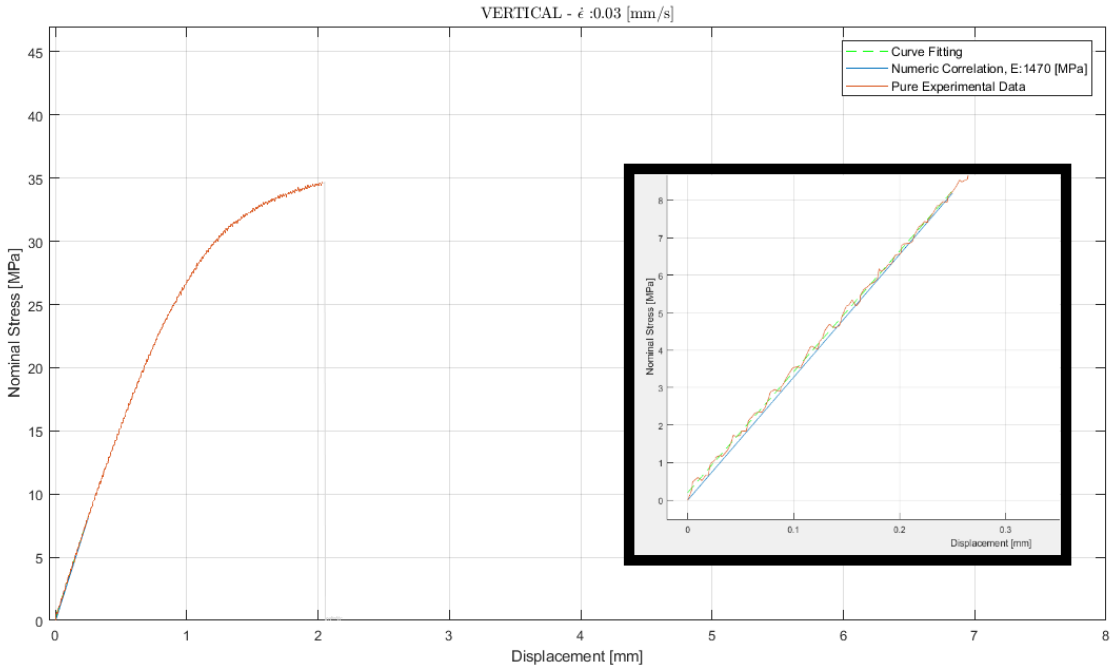

Figure 3-8 *Numerical correlation in elastic region for V_0.03*

The nominal stress vs. displacement graphs with $\dot{\varepsilon} = 0.03\ [mm/s]$ for Horizontal and Vertical specimens can be seen in Figure 3-7 and Figure 3-8. The first order polynomial fitting and the numerical correlations are analogized in elastic region up to 0.5 [mm] and 0.25 [mm], respectively. Because of some lightly non-linear trend of both curves, basically the first order polynomial fitting lines don't start from origin. By considering this, the numerical results were selected as possible as parallel to the fitting lines. As a result of numerical trials in the software, the corresponding Elastic Modulus values are found as 1550 [MPa] and 1470 [MPa]. The values for Elastic Modulus released by the manufacturer were 1600 [MPa] and 1550 [MPa].

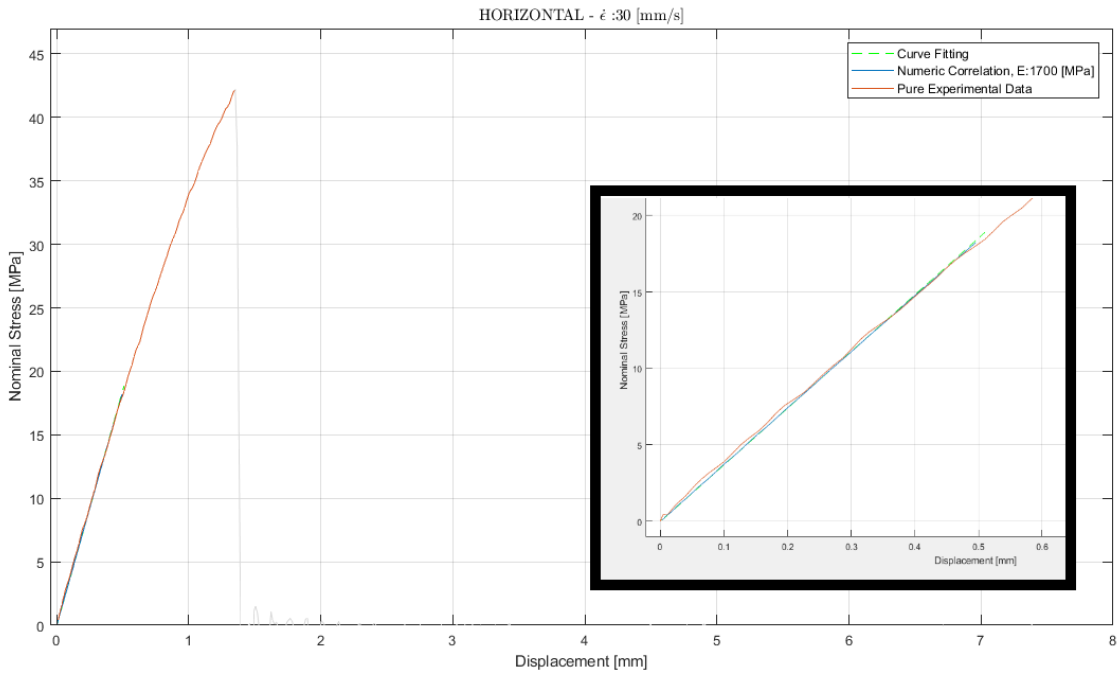

Figure 3-9 *Numerical correlation in elastic region for H_30*

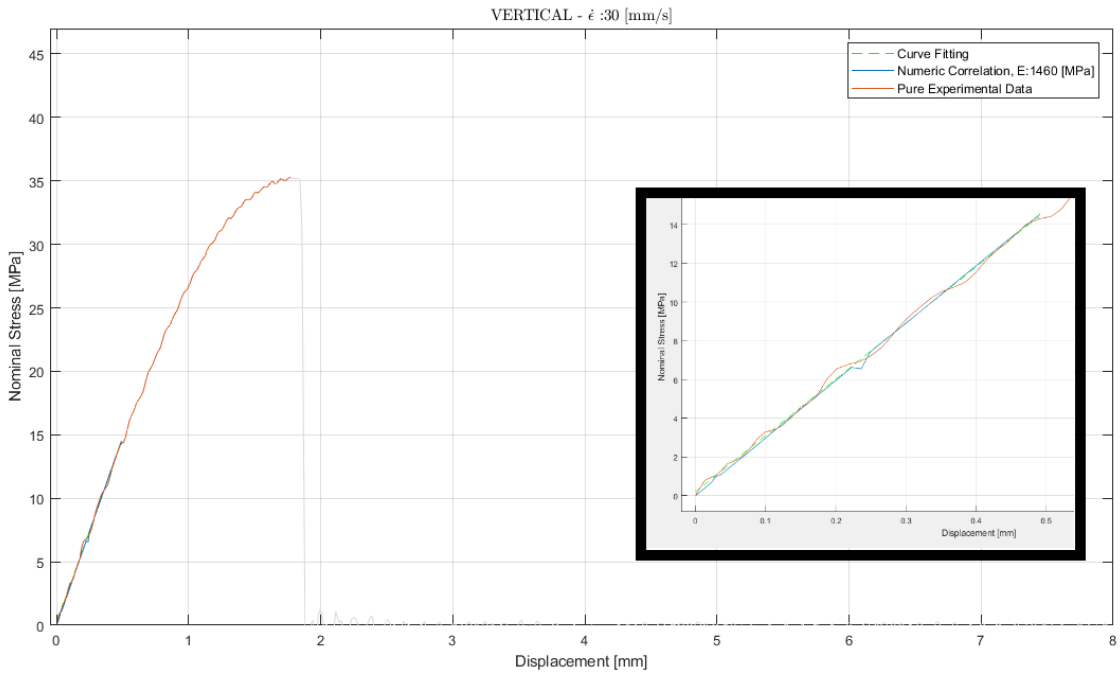

Figure 3-10 *Numerical correlation in elastic region for V_30*

The nominal stress vs. displacement graphs with $\dot{\varepsilon} = 30\ [mm/s]$ for Horizontal and Vertical specimens can be seen in Figure 3-9 and Figure 3-10. The first order polynomial fitting and the numerical correlations are analogized in elastic region up to 0.5 [mm]. The analogy of the first order polynomial fitting lines and the numeric results are almost matched. The corresponding Elastic Moduli are found as 1700 [MPa] for Horizontal and 1460 [MPa] for Vertical specimens.

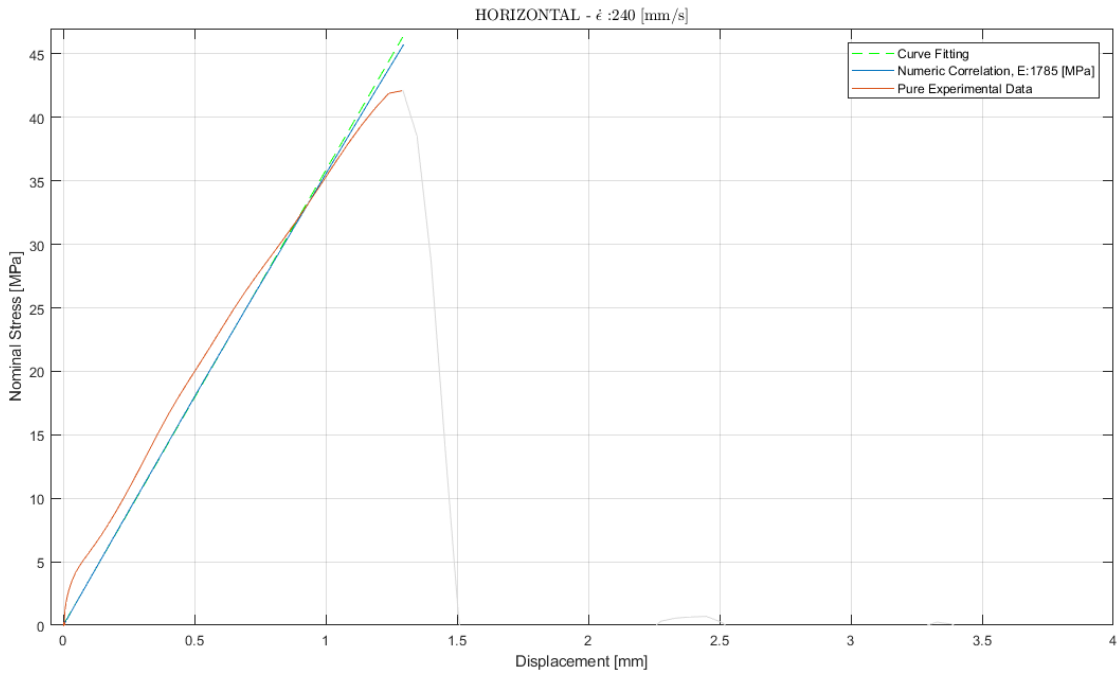

Figure 3-11 *Numerical correlation for H_240*

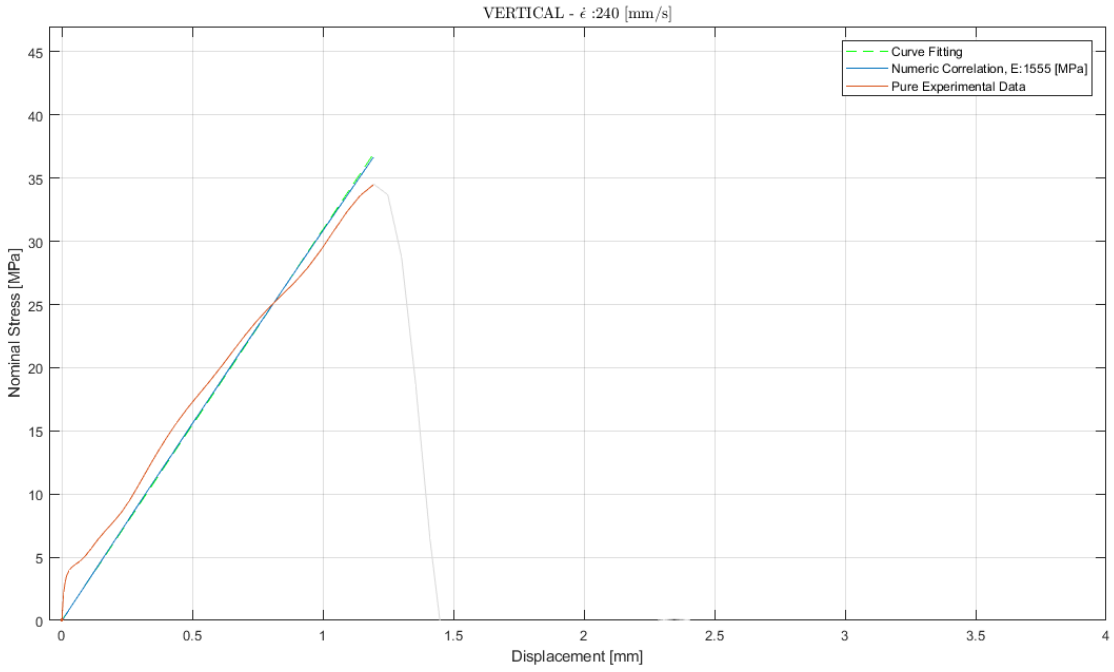

Figure 3-12 *Numerical correlation for V_240*

The above two graphs (Figure 3-11 and Figure 3-12) are with the strain rates $\dot{\varepsilon} = 240\ [mm/s]$ for Horizontal and Vertical specimens. As it can be seen in both graphs, with relatively high strain rates, the material becomes more brittle without having a plastic region. Unlike the previous two strain rate cases, the first order polynomial fitting and the numerical correlations are performed for whole elastic region. The corresponding Elastic Modulus values are found as 1785 [MPa] for Horizontal and 1555 [MPa] for Vertical specimens.

The following Figure 3-13 and Figure 3-14 show for $\dot{\varepsilon} = 480\ [mm/s]$, as the highest strain rate with respect to the others, for Horizontal and Vertical specimens. Generally speaking, the specimens have been broken with less axial displacement with corresponding force values equal or less than the group with $\dot{\varepsilon} = 240\ [mm/s]$. The corresponding Elastic Moduli are found as 1985 [MPa] for Horizontal and 1630 [MPa] for Vertical specimens.

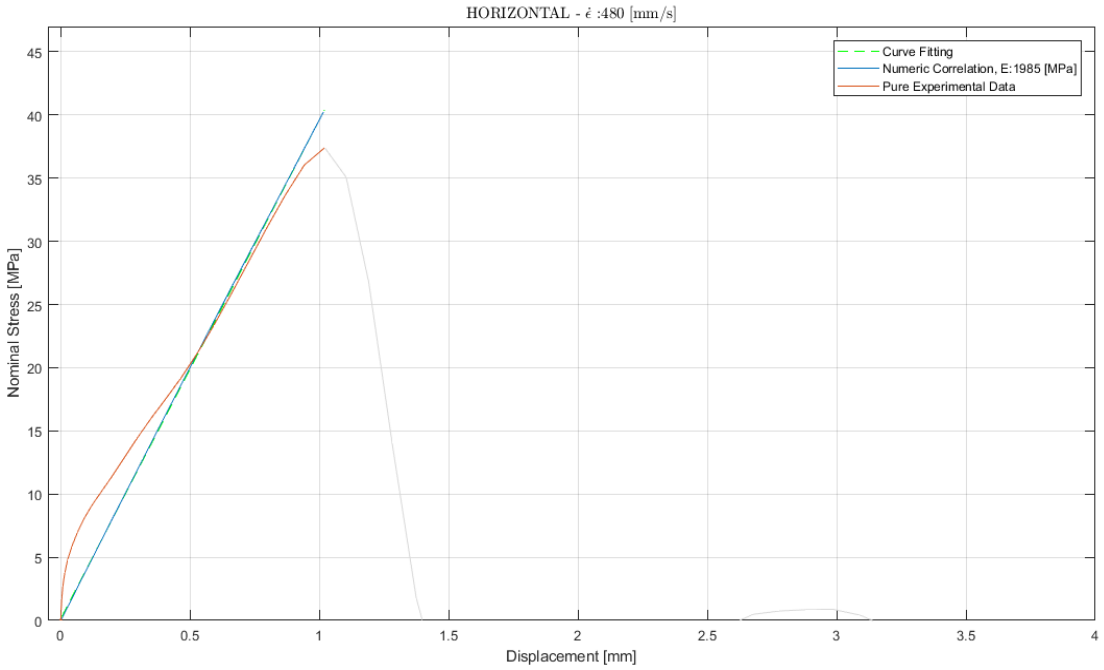

Figure 3-13 *Numerical correlation for V_480*

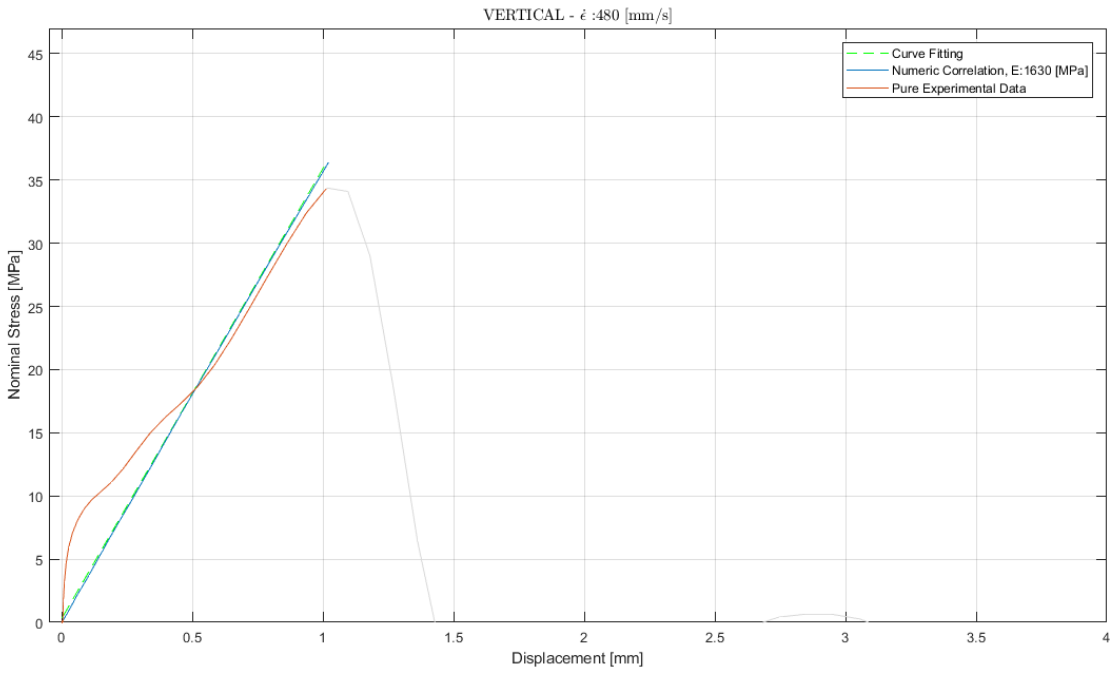

Figure 3-14 *Numerical correlation for V_480*

3.3.2. DETERMINATION OF YIELD STRESSES

After the obtaining the Elastic Moduli for different orientations and strain rates, the next step was to define the Yield Stress values for all cases. In literature, there are some kind of methods to predict the yield stress. In the standard ASTM D638-14, the definition of yield point, where the material starts to yield, is like following; "*the first point on the stress-strain curve at which an increase in strain occurs without an increase in stress*". On the other side, the standard ISO 527-1:2012 Annex A recommends to the users how to perform the slope method for determination of strain at yield with following description; *"… A slope criterion would also involve a moving evaluation interval within which the regression slope of the stress/strain curve is calculated. … Additionally, a criterion must be defined for which slope would be indicative of having found a yield point, for example: Centre-point of the evaluation interval for which the slope becomes negative for the first time.".* As being inspired of these two definitions, the yield stress points are selected by the evaluation slope of stress-strain curves. The yield stresses for both Horizontal and Vertical specimen groups can be seen with following Figure 3-15, Figure 3-16 and Table 3-5.

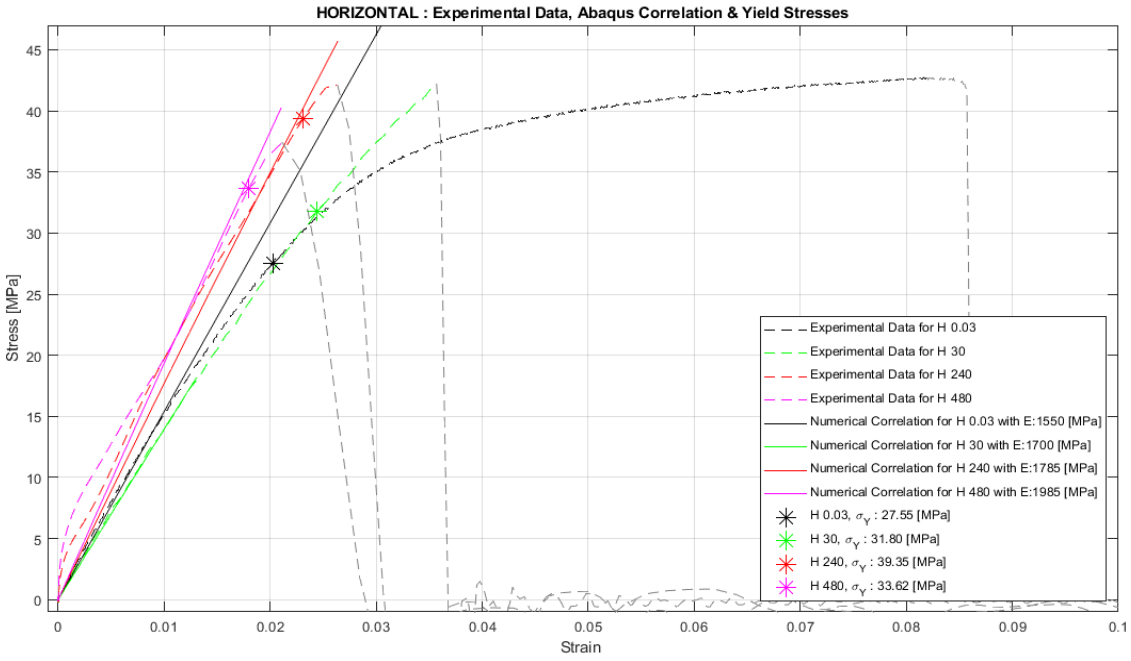

Figure 3-15 *The Yield Stresses for Horizontal specimens*

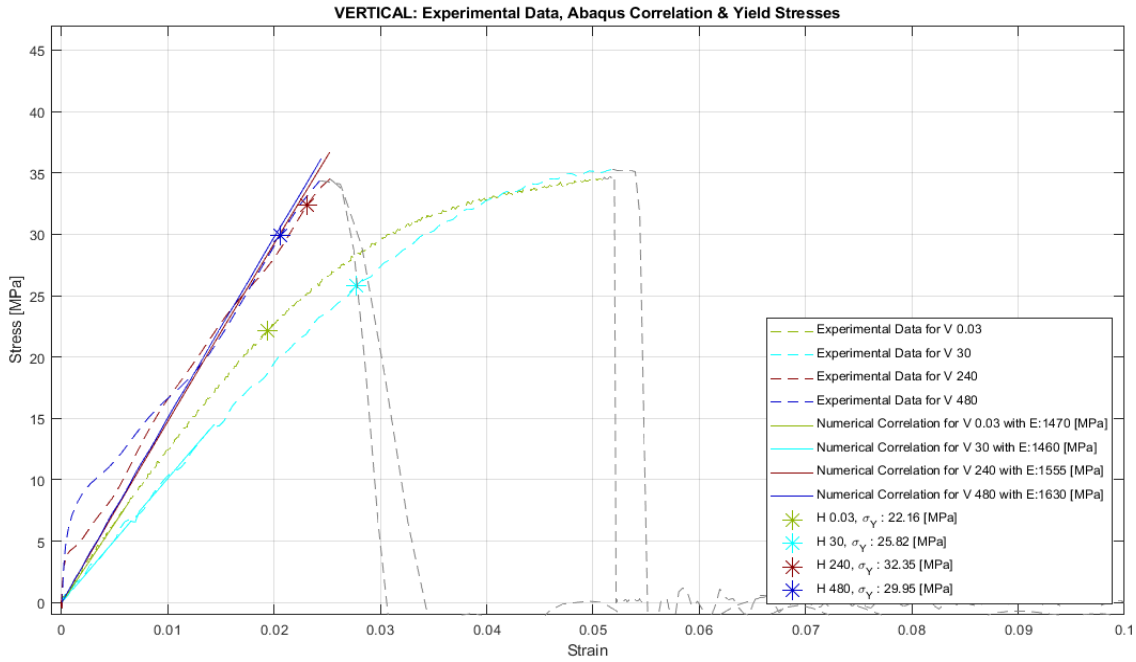

Figure 3-16 *The Yield Stresses for Vertical specimens*

Table 3-5 The Engineering and True Yield Stresses for specimens

SPECIMEN	YIELD STRESS (ENGINEERING) [MPa]	YIELD STRESS (TRUE) [MPa]
H_0.03	27.5451	28.1043
H_30	31.8004	32.5772
H_240	39.3549	40.2637
H_480	33.6176	34.2207
V_0.03	22.1556	22.5851
V_30	25.8245	26.5404
V_240	32.3475	33.0936
V_480	29.9462	30.5633

3.3.3. PLASTIC HARDENING

As the following step in the current work, after the indication of Elastic Moduli for each specimen, the correlation comes to next for whole model including plastic hardening effects. For this aim, there are some methods to define plasticity with plastic hardening algorithms and also the strain rate dependent yielding in literature, and they are known such as *Isotropic Hardening*, *Kinematic Hardening*, *Johnson Cook* or a material subroutine can be defined by user inputs. As primarily, *Johnson Cook* type hardening model is tried to correlate the experimental data. Therefore, some pre-studies performed showed that the correlation doesn't give very suitable fitting with respect to quasi-static tests due to the wide range strain rate tests. Since, this is not the preferred method, the details of this hardening method will not be served.

The preferred method for plastic hardening is one of the basic methodologies, the *Isotropic Hardening,* supported with *Rate Dependent* yielding. As it can be understood, it is needed to define a material's yield behavior accurately for the reason that we have yield strength depends on the rate of straining by taking into account the dynamic effects. To define the rate dependence, *Cowper-Symonds* (*overstress power) law* is decided to perform. The reason to select this type could be explained with following. The number of tests per each specimen were only one and this means that the characteristics of the material at that strain rate is defined with only that test. This situation possibly brings such kind of statistic error. In order to eliminate a possible statistical confusion, the curve fitted by means of mean square error residualization by using Cowper-Symonds Law has been checked in the graphs Yield Stress vs Strain Rate (see Figure 3-17 and Figure 3-18). The flexibility of the Cowper-Symonds law provides that strength model can be used in all element types and in combination with all equations of state and failure properties.

Cowper-Symonds (*overstress power) law* assumes the following relation;

$$R = \frac{\sigma_{Y_D}}{\sigma_{Y_S}} = 1 + \left(\frac{\dot{\varepsilon_{pl}}}{D}\right)^{\frac{1}{n}}$$

where

- $'\sigma_{Y_D}'$ is the dynamic yield stress, depends on the corresponding strain rate
- $'\sigma_{Y_S}'$ is the static yield stress
- 'R' is the simple ratio of $'\frac{\sigma_{Y_D}}{\sigma_{Y_S}}'$
- $'\dot{\varepsilon_{pl}}'$ is the corresponding plastic strain rate
- 'D' and 'n' are the strain rate hardening parameters

The parameters 'D' and 'n' are found by calculation of residuals and minimization by finding minimum of unconstrained multivariable function in MATLAB. Based on the mentioned law, the hardening data for quasi-static cases are used also for dynamic cases with same hardening parameters. The parameters are used during the plastic hardening

are given by following Table 3-6 for Horizontal and Table 3-7 for Vertical specimens. The resulting graphs for the numerical correlation by using Cowper-Symonds Law in plastic hardening can be seen through the Figure 3-19 to Figure 3-22 for Horizontal specimens and through the Figure 3-23 to Figure 3-26 for Vertical specimens.

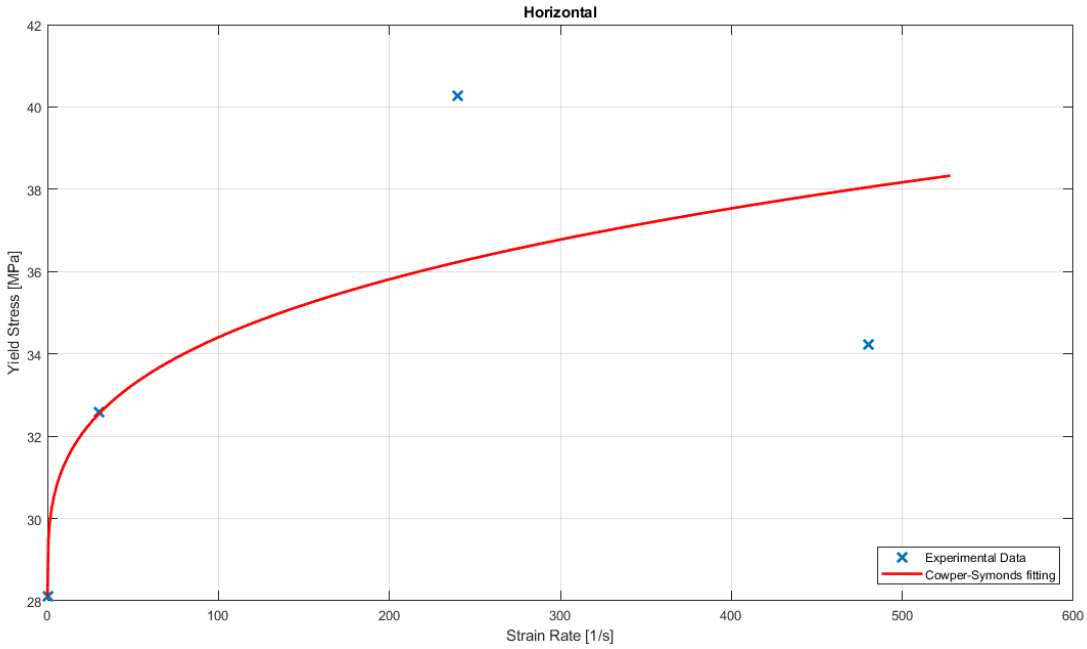

Figure 3-17 *The curve fitting to predict Cowper-Symonds Law parameters 'D' and 'n' as a function of different strain rates based on the R value '1' for quasi-static test for H_0.03*

Table 3-6 *The hardening parameters considered with computation Cowper-Symonds Law for Horizontal specimens*

PARAMETER	$\dot{\varepsilon} = 0.03$ $[mm/s]$	$\dot{\varepsilon} = 30$ $[mm/s]$	$\dot{\varepsilon} = 240$ $[mm/s]$	$\dot{\varepsilon} = 480$ $[mm/s]$
σ_S **[MPa]**	28.1043	-	-	-
σ_D **[MPa]**	-	32.5772	40.2637	34.2207
R	1.000	1.1592	1.4327	1.2176
D	17005			
n	3.434670372471480			

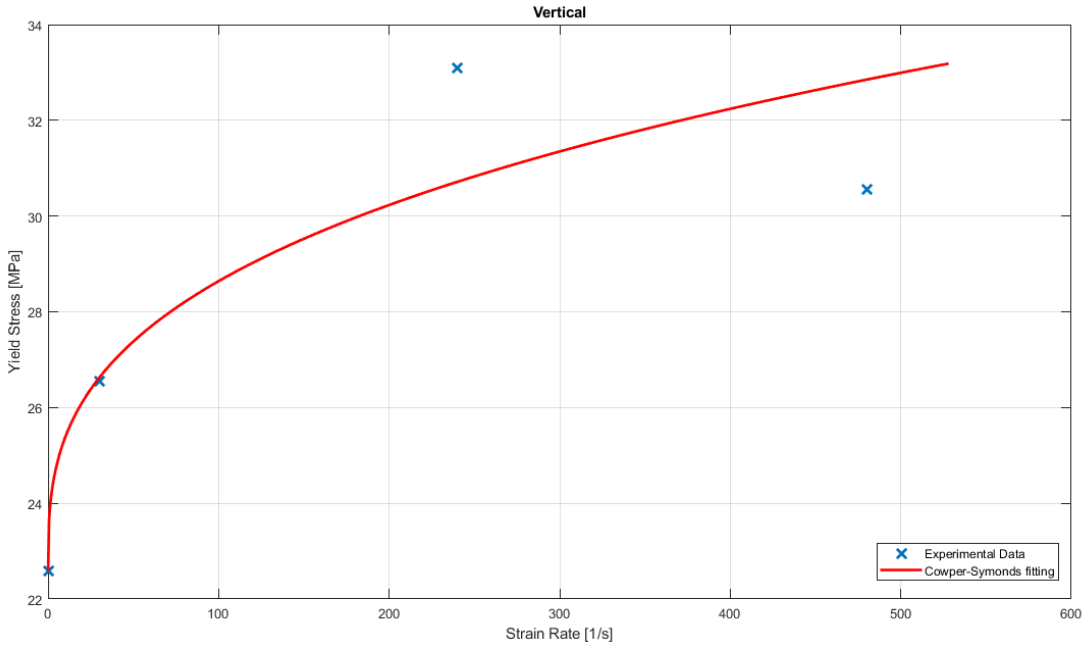

Figure 3-18 *The curve fitting to predict Cowper-Symonds Law parameters 'D' and 'n' as a function of different strain rates based on the R value '1' for quasi-static test for V_0.03*

Table 3-7 *The hardening parameters considered with computation Cowper-Symonds Law for Vertical specimens*

PARAMETER	$\dot{\varepsilon} = 0.03$ $[mm/s]$	$\dot{\varepsilon} = 30$ $[mm/s]$	$\dot{\varepsilon} = 240$ $[mm/s]$	$\dot{\varepsilon} = 480$ $[mm/s]$
σ_S **[MPa]**	22.5851	-	-	-
σ_D **[MPa]**	-	26.5404	33.0936	30.5633
R	1.000	1.1751	1.4653	1.3533
D	5000			
n	2.972523955585784			

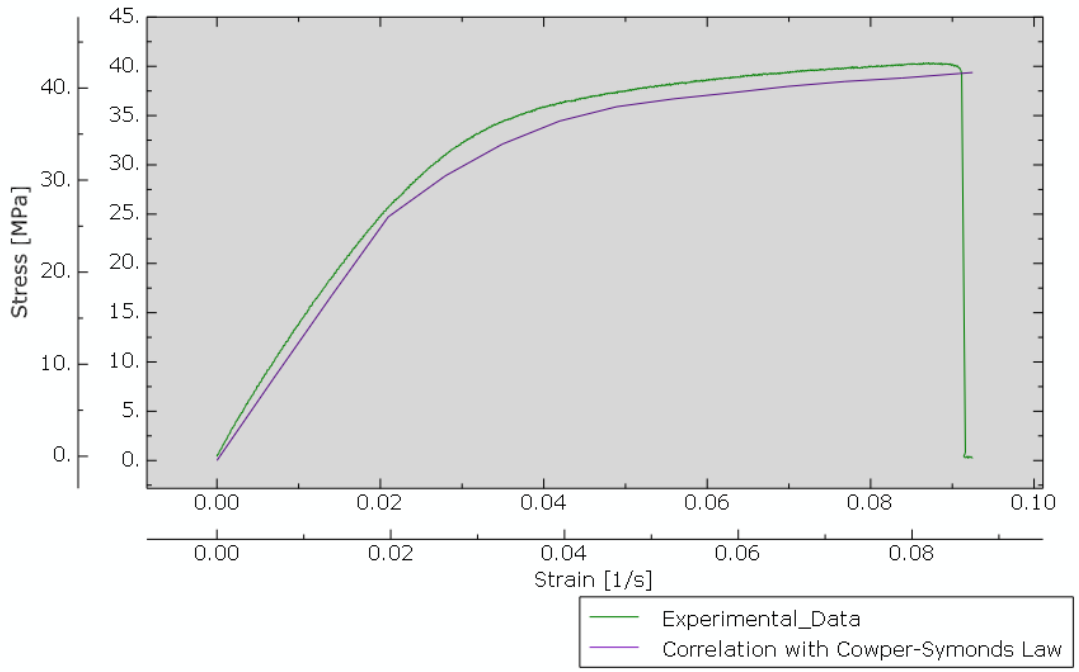

Figure 3-19 *Whole numerical correlation for H_0.03*

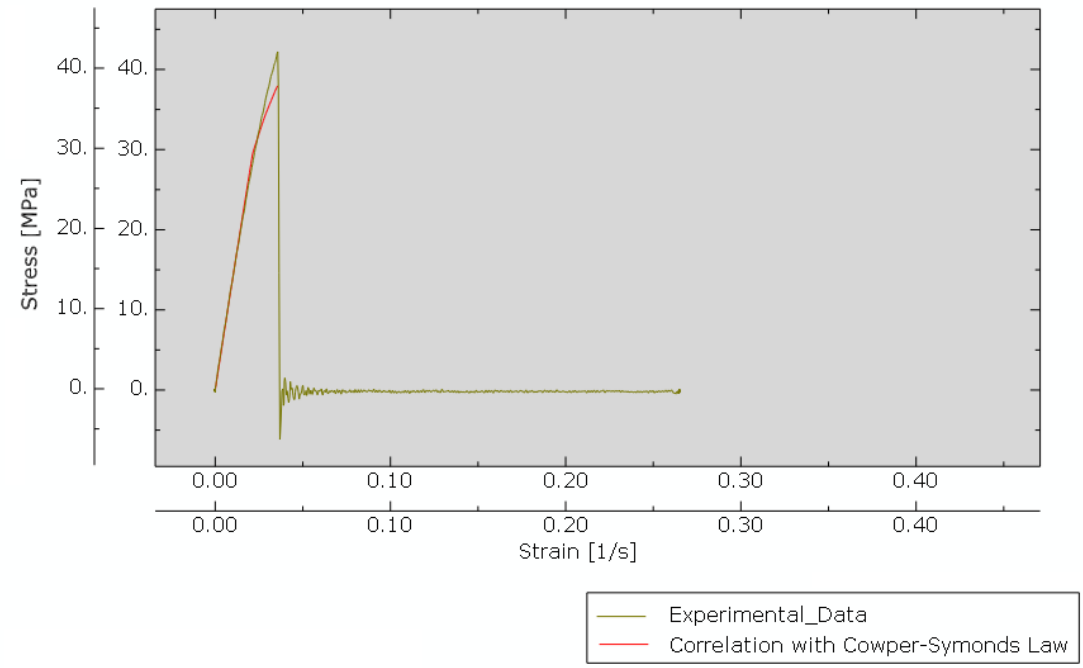

Figure 3-20 *Whole numerical correlation for H_30*

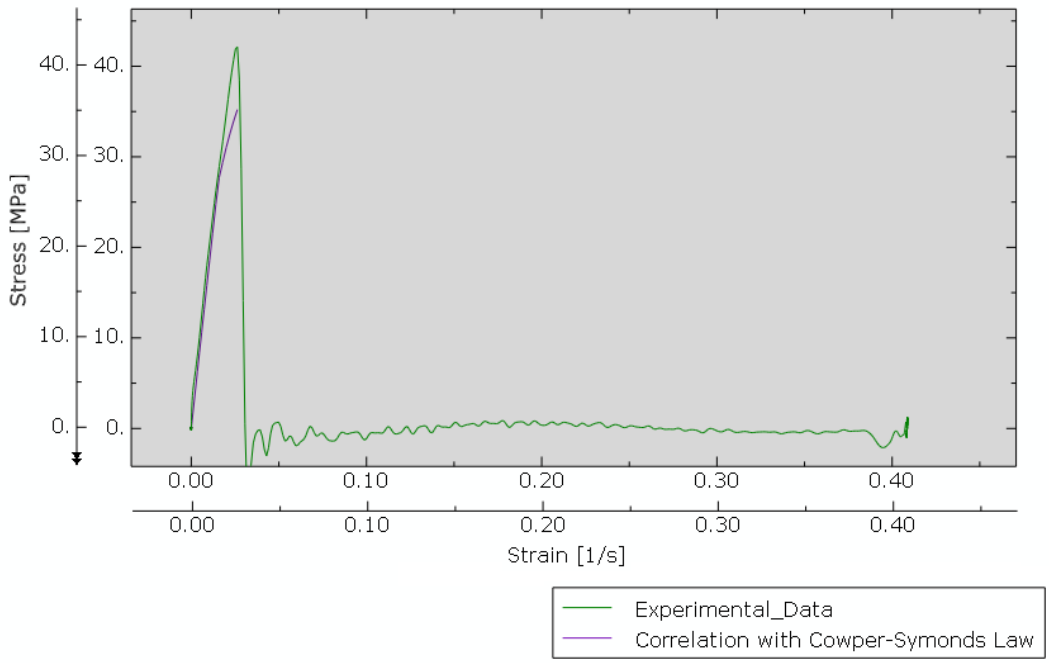

Figure 3-21 *Whole numerical correlation for H_240*

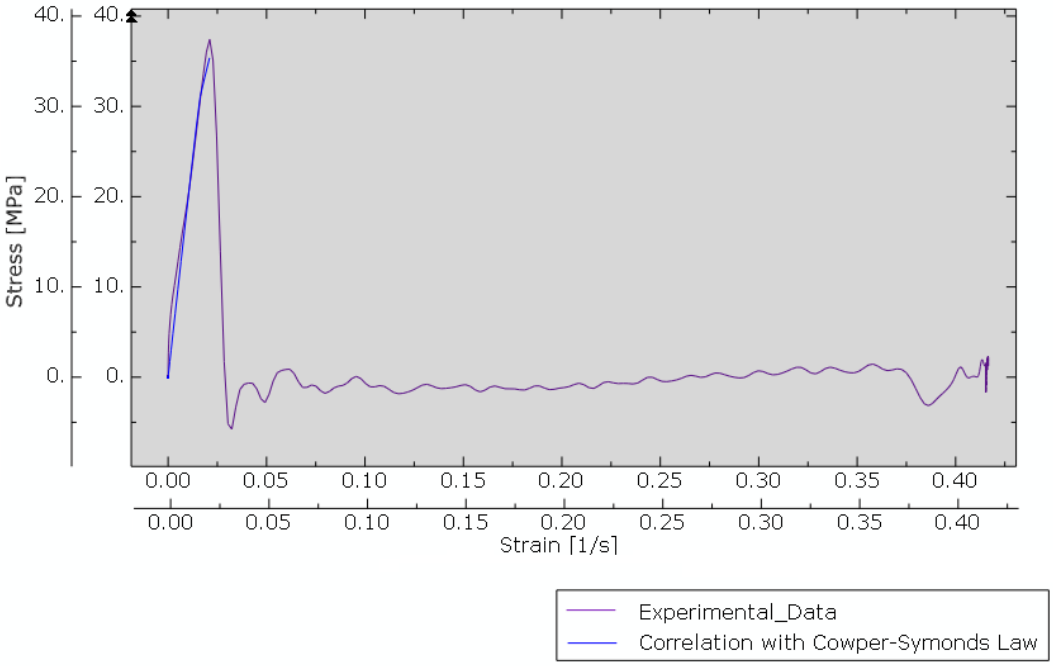

Figure 3-22 *Whole numerical correlation for H_480*

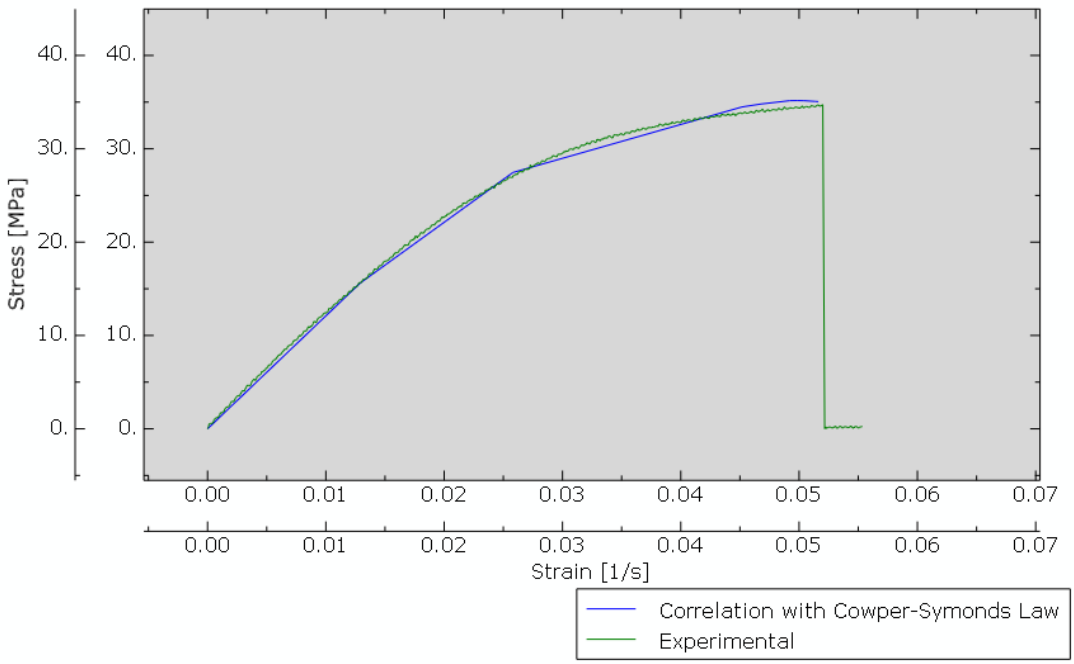

Figure 3-23 *Whole numerical correlation for V_0.03*

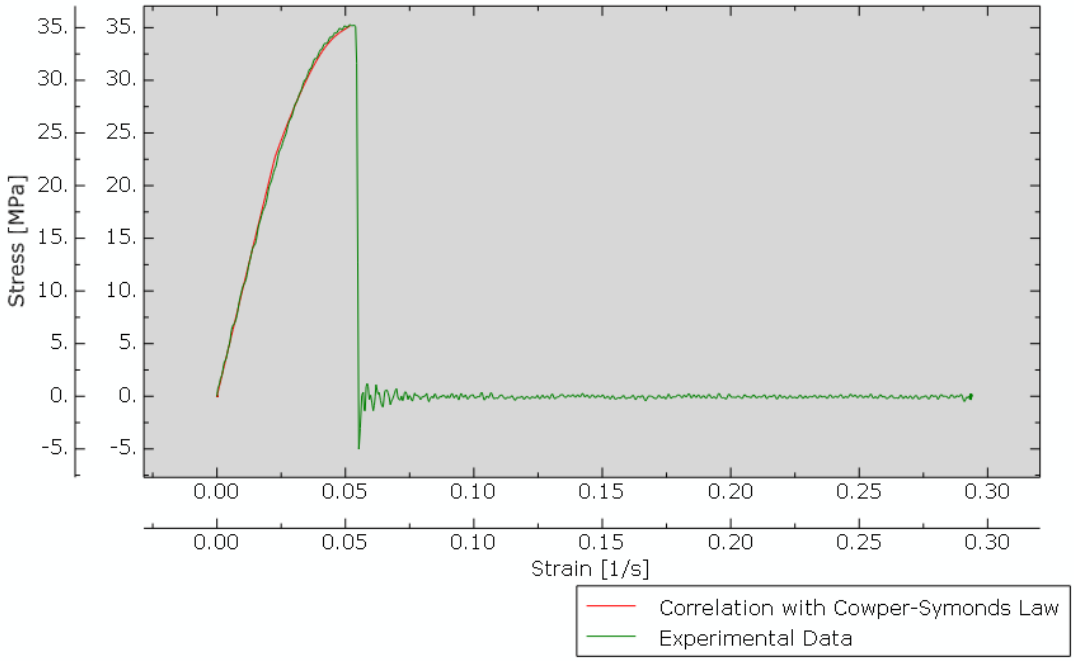

Figure 3-24 *Whole numerical correlation for V_30*

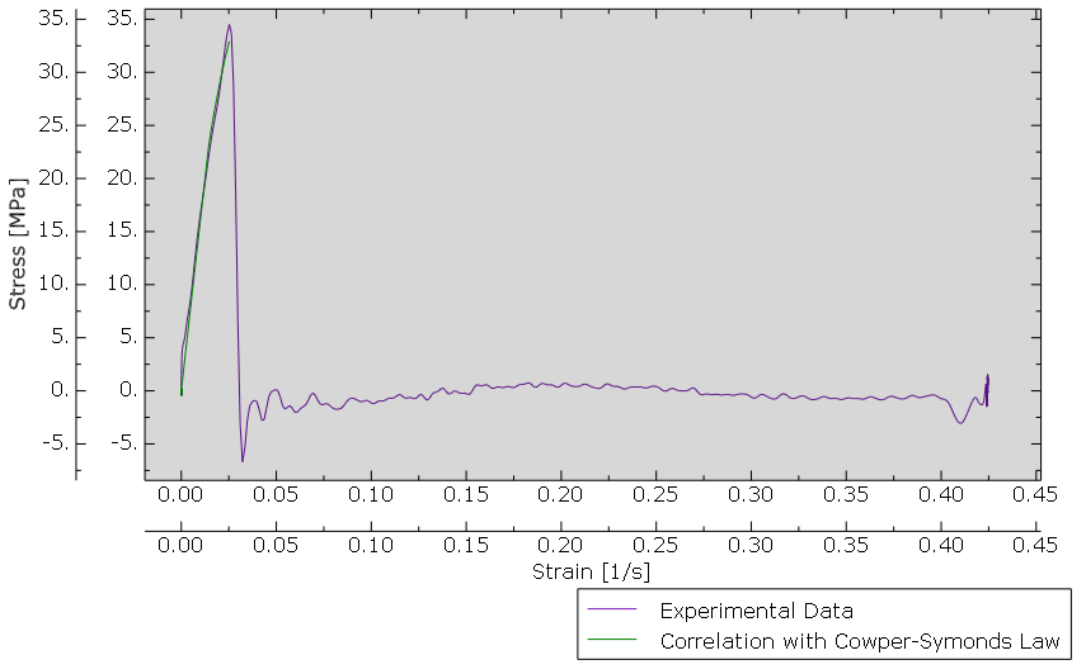

***Figure 3-25** Whole numerical correlation for V_240*

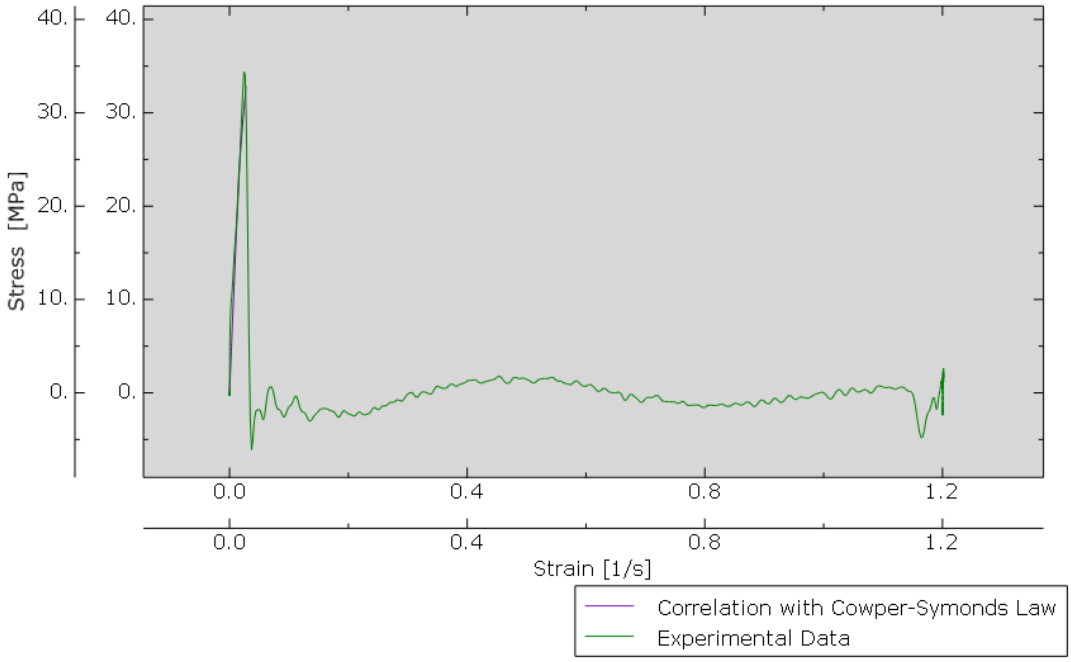

***Figure 3-26** Whole numerical correlation for V_480*

3.3.4. DAMAGE INITIATION AND EVOLUTION

The in-plane crashworthiness of the hexachiral structures is introduced briefly. Based on this scene, a model might be taken into account to predict the progressive damage and failure of the ductile specimens in a general aspect. The ductile damage formulation can be used to model the damage by working on the initiation and evolution as a function of plastic strain.

In this point, it might be useful to see Figure 3-2 to remember how the specimens were broken. While Abaqus/Standard and Abaqus/Explicit offer a general capability for predicting the onset of failure, Abaqus/Explicit offers also a capability for modeling progressive damage and failure of ductile materials. In Abaqus/Explicit, there are some capabilities to predict the damage initiation associated with distinct types of material failure for ductile materials.

Ultimate Tensile Stress (UTS) identifies the material state at the onset of damage, which is referred to as the possibility for the damage initiation. Beyond UTS, the stress-strain response is governed by the evolution of the degradation of the stiffness in the region of strain localization. However, the material stiffness is not degraded in the absence of a damage evolution law. The damage evolution law describes the rate of degradation of the material stiffness once the corresponding initiation criterion has been reached. Consequently, for damage evolution in ductile materials, Abaqus assumes the degraded response that the material would have followed in the absence of damage. In the aim of definition of initiation, the plastic strain at the damage initiation could be introduced by following Table 3-8 for Horizontal specimens and Table 3-9 for Vertical specimens. However, the values given in the table are solely first predictions. Because of the fact the plastic strains computed are the engineering quantities, so that they are averaged on the length L_0, the real plastic strains at the damage initiation shall be significantly higher due to the dependency of the damage to the local effects. In this case, the damage law shall be calibrated by means of FEM. In this present study case, because of the lack of time, unfortunately the damage evaluation could not be performed.

Table 3-8 The UTS and plastic strain at the damage initiation for Horizontal

	UTS [MPa]	PLASTIC STRAIN CORRESPONDS TO UTS
H_0.03	39.3730	0.07152
H_30	37.9423	0.01437
H_240	35.2193	0.01233
H_480	35.3776	0.00473

Table 3-9 The UTS and plastic strain at the damage initiation for Vertical

	UTS [MPa]	PLASTIC STRAIN CORRESPONDS TO UTS
V_0.03	35.0550	0.03872
V_30	35.1750	0.02924
V_240	32.9212	0.01079
V_480	33.6311	0.01475

From this point, since the damage initiation and evolution couldn't be performed completely in the current thesis, the further information can be provided by referring to the Abaqus Analysis User's Guide, Title 24 Progressive Damage and Failure [42].

4. CONCLUSION

The SLS-made PA12 material behavior under uniaxial tensile testing has been examined by considering two main parameters. The one parameter was the material's production orientation. The results showed that the Horizontal orientation reflects the material specifications better than the Vertical orientation. For further similar applications which require reliable results, it is recommended to utilize horizontally manufactured with respect to the powder bed of SLS machine.

The other parameter was the strain rate, changing from 0.03 [mm/s] to 480 [mm/s] as representative of one quasi-static and three dynamic tests. In dynamic tests, both Vertical and Horizontal oriented specimens showed a brittle behavior than estimated. As the strain rate increase, specimens have reached to UTS at relatively lower strains. However, the number of the tests were not enough to state about a consistent comparison for yield stresses.

Moreover, considering the limited number of experiments, FEM also introduced simultaneously. Numerical correlations in elastic region are introduced by a linear fitting, while the plastic hardenings are performed with the guidance of tabular data obtained from quasi-static results and hardening parameters by using Cowper-Symonds Law defined in rate dependence for isotropic hardening. Consequently, successful correlations are obtained.

5. BIBLIOGRAPHY

[1] L. l. LIN, Y. s. SHI, F. d. ZENG and S. h. HUANG, "Microstructure of Selective Laser Sintered Polyamide," *Journal of WuhanUniversityof Technology - Mater.Sci.Ed.*, vol. 18, no. 3, 2003.

[2] A. AIROLDI, P. BETTINI, P. PANICHELLI, M. F. OKTEM and G. SALA, "Chiral topologies for composite - Part I: Development of a chiral rib for deformable airfoils," *Phys. Status Solidi B*, vol. 252, no. 7, p. 1435–1445, 2015.

[3] J. GRIMA, R. GATT and P. S. FARRUGIA, "On the properties of auxetic meta-tetrachiral structures," *Phys. Status Solidi B*, vol. 245, no. 3, pp. 511-520, 2008.

[4] A. BACIGALUPO and L. GAMBAROTTA, "Simplified modelling of chiral lattice materials with local resonators," *International Journal of Solids and Structures*, vol. 83, pp. 126-141, 2016.

[5] A. AIROLDI, M. CRESPI, G. QUARANTA and G. SALA, "Design of a Morphing Airfoil with Composite Chiral Structure," *JOURNAL OF AIRCRAFT*, vol. 49, no. 4, pp. 1008-1019, 2012.

[6] A. AIROLDI, P. BETTINI, M. BOIOCCHI and G. QUARANTA, "Composite Elements for Biomimetic Aerospace Structures with Progressive Shape Variation Capabilities," *Advances in Technology Innovation*, vol. 1, no. 1, pp. 13-15, 2016.

[7] P. BETTINI, A. AIROLDI, G. SALA, L. DI LANDRO, M. RUZZENE and A. SPADONI, "Composite chiral structures for morphing airfoils: Numerical analyses and development of a manufacturing process," *Composites*, vol. 41, no. Part B, pp. 133-147, 2010.

[8] A. AIROLDI, P. BETTINI, P. PANICHELLI and G. SALA, "Chiral topologies for composite morphing structures – Part II: Novel configurations and technological processes," *Phys. Status Solidi B*, vol. 252, no. 7, p. 1446–1454, 2015.

[9] D. BORNENGO, F. SCARPA and C. REMILLAT, "Evaluation of hexagonal chiral structure for morphing airfoil concept," *Journal of Aerospace Engineering*, vol. 219, no. 3, pp. 185-192, 2005.

[10] W. MILLER, C. W. SMITH, F. SCARPA and K. E. EVANS, "Flatwise buckling optimization of hexachiral and tetrachiral honeycombs," *Composites Science and Technology*, vol. 70, no. 7, pp. 1049-1056, 2010.

[11] A. AIROLDI, P. BETTINI, M. ZAZZARINI and F. SCARPA, "Failure and energy absorption of plastic and composite chiral honeycombs," in *Structures Under Shock and Impact XII*, WIT PRESS, 2013, pp. 101-114.

[12] A. ALDERSON, K. L. ALDERSON , N. RAVIR, N. RAVIRALA and K. M. ZIED, "The in-plane linear elastic constants and out-of-plane bending of 3-coordinated ligament and cylinder-ligament honeycombs," *Composites Science and Technology,* vol. 70, pp. 1034-1041, 2010.

[13] A. ALDERSON, K. L. ALDERSON, D. ATTARD, K. E. EVANS, R. GATT, J. N. GRIMA, W. MILLER, N. RAVIRALA, C. W. SMITH and K. ZIED, "Elastic constants of 3-, 4- and 6-connected chiral and anti-chiral honeycombs subject to uniaxial in-plane loading," *Composites Science and Technology,* vol. 70, no. 7, pp. 1042-1048, 2010.

[14] D. ZHANG, F. QINGGUO and P. ZHANG, "In–plane dynamic crushing behavior and energy absorption of honeycombs with a novel type of multi-cells," *Thin-Walled Structures,* vol. 117, pp. 199-210, 2017.

[15] D. RUAN, G. LU, B. WANG and T. X. YU, "In-plane dynamic crushing of honeycombs - a finite element study," *International Journal of Impact Engineering,* vol. 28, pp. 161-182, 2003.

[16] S. D. PAPKA and S. KYRIAKIDES, "Biaxial crushing of honeycombs - Part I: Experiments," *International Journal of Solids and Structures,* vol. 36, pp. 4367-4396, 1999.

[17] S. D. PAPKA and S. KYRIAKIDES, "In-plane biaxial crushing of honeycombs - Part II: Analysis," *International Journal of Solids and Structures,* vol. 36, pp. 4397-4423, 1999.

[18] D. GAO and C. W. ZHANG, "In-plane crashworthiness of chiral honeycombs," in *MECHANICS OF STRUCTURES AND MATERIALS: ADVANCEMENTS AND CHALLENGES*, vol. 1, London, CRC Press, 2017, pp. 889-894.

[19] C. YAN, L. HAO, L. XU and Y. SHI, "Preparation, characterisation and processing of carbon fibre/polyamide-12 composites for selective laser sintering," *Composites Science and Technology,* vol. 71, pp. 1834-1841, 2011 .

[20] M. SCHMIDT, D. POHLE and T. RECHTENWALD, "Selective Laser Sintering of PEEK," *CIRP Annals,* vol. 56, no. 1, pp. 205-208, 2007.

[21] S. SINGH, V. S. SHARMA, A. SACHDEVA and S. K. SINHA, "Optimization and Analysis of Mechanical Properties for Selective Laser Sintered Polyamide Parts," *Materials and Manufacturing Processes,* vol. 28, no. 2, pp. 163-172, 2013.

[22] R. GOODRIDGE, R. J. M. HAGUE and C. J. TUCK, "Effect of long-term ageing on the tensile properties of a polyamide 12 laser sintering material," *Polymer Testing,* vol. 29, no. 4, pp. 483-493, 2010.

[23] R. GOODRIGDE, C. J. TUCK and R. J. M. HAGUE, "Laser sintering of polyamides and other polymers," *Progress in Materials Science*, vol. 57, no. 2, pp. 229-267, 2012.

[24] S. KUMAR and A. CZEKANSKI, "Development of filaments using selective laser sintering waste powder," *Journal of Cleaner Production*, vol. 165, pp. 1188-1196, 2017.

[25] S. GRIESSBACH, R. LACH and W. GRELLMANN, "Small series production of high-strength plastic parts," *Kunststoffe International,* vol. 98, no. 5, pp. 11-14, 2008.

[26] VIRGINA TECH UNIVERSITY, "DREAMS," [Online]. Available: http://seb199.me.vt.edu/dreams/laser-sintering/.

[27] A. AMADO-BACKER, J. RAMOS-GREZ, M. J. YANEZ, Y. VARGAS and L. GAETE-GARRETON, "Elastic tensor stiffness coefficients for SLS Nylon 12 under different degrees of densification as measured by ultrasonic technique," *Rapid Prototyping Journal*, vol. 14, no. 5, pp. 260-270, 2008.

[28] N. HOPKINSON, C. E. MAJEWSKI and H. ZARRINGHALAM, "Quantifying the degree of particle melt in Selective Laser Sintering®," *CIRP Annals*, vol. 58, no. 1, pp. 197-200, 2009.

[29] B. CAULFIELD, P. E. McHUGH and S. LOHFELD, "Dependence of mechanical properties of polyamide components on build parameters in the SLS process," *Journal of Materials Processing Technology*, vol. 182, pp. 477-488, 2007.

[30] G. d. O. SETTI, M. F. de OLIVEIRA, I. A. MAIA, J. V. LOPES da SILVA, R. SAVU and E. JOANNI, "Correlation between mechanical and surface properties of SLS parts," *Rapid Prototyping Journal*, vol. 20, no. 4, pp. 285-290, 2014.

[31] M. BLATTMEIER, G. WITT, J. WORTBERG, J. EGGERT and J. TOEPKER, "Influence of surface characteristics," *Rapid Prototyping Journal*, vol. 18, no. 5, pp. 161-171, 2012.

[32] A. WEGNER, R. HARDER, G. WITT and D. DRUMMER, "Determination of Optimal Processing Conditions for the Production of Polyamide 11 Parts using the Laser Sintering Process," *International Journal of Recent Contributions from Engineering, Science & IT*, vol. 3, no. 1, pp. 5-12, 2015.

[33] T. STICHEL, T. FRICK, T. LAUMER, F. TENNER, T. HAUSOTTE, M. MERKLEIN and M. SCHMIDT, "A Round Robin study for Selective Laser Sintering of polyamide 12: Microstructural origin of the mechanical properties," *Optics & Laser Technology*, vol. 89, pp. 31-40, 2017.

[34] E. C. HOFLAND, I. BARAN and D. A. WISMEIJER, "Correlation of Process Parameters with Mechanical Properties of Laser Sintered PA12 Parts," *Advances in Materials Science and Engineering*, vol. 2017, no. 4953173, p. 11 pages, 2017.

[35] E. MOESKOPS, N. KAMPERMAN, B. van de VORST and R. KNOPPERS, "CREEP BEHAVIOUR OF POLYAMIDE IN SELECTIVE LASER SINTERING," TNO Industrial Technology , Eindhoven, 2004.

[36] N. LAMMENS, M. KERSEMANS, I. DE BAERE and W. VAN PAEPEGEM, "On the visco-elasto-plastic response of additively manufactured polyamide-12 (PA-12) through selective laser sintering," *Polymer Testing*, vol. 57, pp. 149-155, 2017.

[37] U. AJOKU, N. SALEH, N. HOPKINSON, R. HAGUE and P. ERASENTHIRAN, "Investigating mechanical anisotropy and end-of-vector effect in," *Journal of Engineering Manufacture*, vol. 220, no. 7, pp. 1077-1086, 2006.

[38] EOS, "Material Data Center," EOS, [Online]. Available: https://eos.materialdatacenter.com/eo/standard/main/ds.

[39] P. LAMBERT, "Sculpteo," 14 May 2014. [Online]. Available: https://www.sculpteo.com/blog/2014/05/14/right-plastic-production-method-part-3/.

[40] MTS SYSTEMS CORPORATION, "Universitat Politècnica de Catalunya - BarcelonaTech (UPC)," 2006. [Online]. Available: https://www.upc.edu/sct/en/documents_equipament/d_77_id-412.pdf.

[41] NIKON, "Nikon Digital Camera 1 J5 Reference Manual," 2015. [Online]. Available: http://download.nikonimglib.com/archive2/KHQwO00QyCaO010Bia9982yA7991/1J5RM_(En)02.pdf.